Traveling waves and breathers in an excitatory-inhibitory neural field

Stefanos E. Folias*

Department of Mathematics & Statistics, University of Alaska Anchorage, Anchorage, Alaska 99508, USA

(Received 14 October 2016; revised manuscript received 15 February 2017; published 13 March 2017)

We study existence and stability of traveling activity bump solutions in an excitatory-inhibitory (E-I) neural field with Heaviside firing rate functions by deriving existence conditions for traveling bumps and an Evans function to analyze their spectral stability. Subsequently, we show that these existence and stability results reduce, in the limit of wave speed $c \to 0$, to the equivalent conditions developed for the stationary bump case. Using the results for the stationary bump case, we show that drift bifurcations of stationary bumps serve as a mechanism for generating traveling bump solutions in the E-I neural field as parameters are varied. Furthermore, we explore the interrelations between *stationary* and *traveling* types of *bumps* and *breathers* (time-periodic oscillatory bumps) by bridging together analytical and simulation results for stationary and traveling bumps and their bifurcations in a region of parameter space. Interestingly, we find evidence for a codimension-2 drift-Hopf bifurcation occurring as two parameters, inhibitory time constant τ and I-to-I synaptic connection strength $\bar{w}_{ii}$, are varied and show that the codimension-2 point serves as an organizing center for the dynamics of these four types of spatially localized solutions. Additionally, we describe a case involving subcritical bifurcations that lead to traveling waves and breathers as τ is varied.

DOI: 10.1103/PhysRevE.95.032210

I. INTRODUCTION

Traveling waves of activity have been observed in a variety of brain regions under different conditions [1–13] and also in brain slice preparations [1,14,15]. Synaptic inhibition is known to control the spread of excitation, yet propagating waves of activity can occur in the presence of robust inhibition [1]. Theoretical results from neural fields have already begun to show successful control of wave propagation in cortical slice experiments [15].

Neural fields are spatially extended nonlinear integrodifferential equations that represent the large-scale dynamics of populations of neurons mediated by synaptic interactions and other neuronal processes (e.g., firing rate adaptation and synaptic depression) and support a wide range of spatiotemporal dynamics, including traveling waves [16–20]. Two variations on the original excitatory-inhibitory (E-I) neural field introduced in [16] that employ the Heaviside firing rate simplification [21] have been studied by Pinto and Ermentrout [22] and Blomquist *et al.* [23]; our work herein concerns the latter.

Traveling waves in neural fields have been examined in a variety of contexts, including neural fields with adaptation [24–30], asymmetric connectivity [31], synaptic depression [32,33], refractoriness [34], transmission delays [35,36], recurrent inhibition [37], spatial inhomogeneities and horizontal connections [38–41], and noise [42,43]. Spectral stability of traveling waves can be analyzed with an Evans function, which was initially developed for neural fields in [25] and has been calculated and used in neural fields where threshold conditions occur in only one neuronal population [26–28,30] or in a pair of interacting neural fields but in the simpler case of traveling fronts [42] which reduces the number of threshold crossings that the wave depends on nonlinearly. Drift bifurcations—wherein stationary bumps destabilize and give rise to traveling waves—have been briefly examined in a neural field with nonlinear adaptation [44] and an interacting pair of E-I neural fields [45] and in more detail in [46–48]. Hopf bifurcations of stationary bumps have been studied in various neural fields [22,23,44,49–52] and can produce different forms of stationary oscillatory activity bumps, e.g., *stationary breathers*. It is also possible for localized traveling waves to undergo Hopf bifurcations that give rise to stable temporally oscillating traveling waves. Such waves occur both in neural fields, taking the form of *traveling breathers* [27], and also in synaptically connected spiking neuronal networks, where they can take the form of *lurching waves* [53].

Studies of traveling waves of activity in various formulations of E-I neural fields are limited and have primarily examined numerical simulations only [16,45,54,55]. Amari developed existence conditions for traveling waves analytically in the special case of an E-I neural field wherein the I population dynamics at location x is governed by synaptic inputs from the E and I populations at location x only [21], which shares some aspects with the adaptation variable in the model of Pinto and Ermentrout [24]. Thus, while each point in the E population receives inhibition from many locations x, the synaptic inhibition from each location x is determined solely by the local E-I population at x; consequently, wave existence is determined by the threshold conditions in the E population only. To contrast, the E-I neural field considered herein allows synaptic inputs (afferents) to both E and I populations to arise from populations at any location in space (or feature space), and wave existence is determined by threshold conditions in both E and I populations.

In this paper, we develop existence and stability conditions for traveling bumps in a general E-I neural field. One difference from previous studies is that traveling bump existence in the neural field here requires solving a four-dimensional (4D) nonlinear system of equations rather than a 2D system. The organization of the paper is as follows. We begin by introducing the E-I neural field model (1) and some assumptions upon it. In Sec. II, we develop existence conditions for a traveling bump

*sfolias@alaska.edu

solution and an expression for the traveling bump profile that are valid for both cases of (i) no input and (ii) a traveling bump that is locked to a localized input traveling with constant speed. Subsequently we compare results of numerical simulations of the E-I neural field with those of the existence conditions. In Sec. III, we analyze the spectral stability of traveling bump solutions, derive an Evans function to calculate their stability, and compare its results with numerical simulations. In Sec. IV, we examine the reduction in limit as wave speed $c \to 0$ for both cases of the existence conditions and the Evans function. In Sec. V, we discuss the drift bifurcation as a mechanism for traveling bump generation, and combine a mixture of existence, stability, bifurcation, and numerical simulation results for both stationary and traveling bumps to examine their behavior and interrelation with stationary and traveling breathers extensively in a particular region of parameter space. Finally, in Sec. V F we examine a different example of traveling wave and traveling breather generation resulting from subcritical bifurcations in a different region of parameter space.

We consider excitatory-inhibitory (E-I) neural field [23],

$$\begin{aligned} \frac{\partial u_e}{\partial t} + u_e &= w_{ee} * f_e(u_e) - w_{ei} * f_i(u_i) + I_e, \\ \tau \frac{\partial u_i}{\partial t} + u_i &= w_{ie} * f_e(u_i) - w_{ii} * f_i(u_i) + I_i, \end{aligned} \tag{1}$$

posed on the space $C^1_{\text{unif}}(\mathbb{R},\mathbb{R}^2)$ where $\tau > 0$ is the relative inhibitory time constant, $I_j(x,t)$ represent inputs, the nonlinearities f_j are Heaviside functions of the form

$$f_j(u) \;=\; H(u-\theta_j), \quad j \in \{e,i\},$$

$\theta_{e,i}$ denote the thresholds for excitatory and inhibitory populations, respectively, and $w_{jk} * f_k(u)$ is expressed as

$$[w_{jk} * f_k(u)](x,t) = \int_{-\infty}^{\infty} w_{jk}(x-y) H[u_k(y,t) - \theta_k] dy.$$

Synaptic weight distributions $w_{jk}(x)$ for $j,k \in \{e,i\}$ are assumed to be positive, even-symmetric, continuously differentiable functions and integrable over $(-\infty,\infty)$. In a related neural field, spectral stability was shown to imply nonlinear stability when posed on the space $C^1_{\text{unif}}(\mathbb{R},\mathbb{R}^2)$ with $w_{jk}(x) \in C^1_{\text{unif}}(\mathbb{R},\mathbb{R}) \cap W^{1,1}(\mathbb{R},\mathbb{R})$ [30].

E-I neural field (1) is a mean field model that treats neural tissue as a spatial continuum (or a continuum in some feature space) where $u_e(x,t)$ and $u_i(x,t)$ represent the activity of the population of excitatory and inhibitory neurons, respectively, at location x and time t. Neural fields are amenable to modeling areas of the neocortex due to their layered structure of networks of excitatory and inhibitory neurons with approximate regular patterns of space-dependent and feature-dependent synaptic connections. A layer of neural tissue can be collapsed to a two-dimensional sheet if the activity is approximately uniform along vertical lines through the layer, e.g., due to strong vertical connections. Neural field (1) represents a layer of excitatory and inhibitory neurons *in vivo* or *in vitro*, with intralayer synaptic connections w_{jk} assumed to be isotropic and distance dependent, reflecting, to a first approximation, the short-range connections to both excitatory and inhibitory neurons in various regions of cortex. The two-dimensional layer here is further reduced to a one-dimensional layer for simplicity; however, all of the solutions studied herein have natural localized two-dimensional analogs. Inputs $I_{e,i}(x,t)$ to the E and I populations can be construed in various ways, such as external current inputs from electrodes, or prescribed synaptic input from a different pool of neurons within the same or different layer (or different brain region), or reflecting regions where neurons are more depolarized or activity is modulated by other prescribed processes.

II. EXISTENCE CONDITIONS FOR TRAVELING BUMP SOLUTIONS

We seek traveling bump solutions of the form $(u_e(x,t),u_i(x,t)) = (V_e(\xi),V_i(\xi))$ where $\xi = x - ct$ is the traveling wave coordinate, c is the wave speed, and

$$V_e(\xi)\begin{cases} > \theta_e & \xi \in (\xi_0^e,\xi_1^e) \\ = \theta_e & \xi = \xi_0^e,\xi_1^e \\ < \theta_e & \text{otherwise} \end{cases}, \tag{2}$$

$$V_i(\xi)\begin{cases} > \theta_i & \xi \in (\xi_0^i,\xi_1^i) \\ = \theta_i & \xi = \xi_0^i,\xi_1^i \\ < \theta_i & \text{otherwise} \end{cases}. \tag{3}$$

When $I_{e,i}(x,t) = 0$, neural field (1) is translation invariant and, without loss of generality, we can set $\xi_0^e = 0$ with the wave speed c and the threshold boundaries ξ_1^e,ξ_0^i,ξ_1^i selected by the network. In the separate case of a traveling bump locked to a traveling localized input $I_j(x,t) = I_j(x-ct)$, the speed c of the bump is assumed to match the prescribed speed of the input. Translation symmetry is broken by the input inhomogeneity and the four threshold boundaries $\xi_0^e,\xi_1^e,\xi_0^i,\xi_1^i$ instead are determined by the network and depend on the position of the input in the traveling coordinate frame ξ.

In either case, a traveling bump solution (V_e,V_i) satisfies the following equation in traveling wave coordinates:

$$\begin{aligned} -c\frac{\partial V_e}{\partial \xi} + V_e &= w_{ee} * f_e(V_e) - w_{ei} * f_i(V_i) + I_e(\xi), \\ -c\tau\frac{\partial V_i}{\partial \xi} + V_i &= w_{ie} * f_e(V_e) - w_{ii} * f_i(V_i) + I_i(\xi) \end{aligned} \tag{4}$$

together with the threshold conditions (2) and (3). The nonlinear terms of the traveling bump (V_e,V_i) in (4) may be expressed as explicit functions ($\mathcal{W}_e$ and $\mathcal{W}_i$) of the threshold boundaries of the activity bump, ξ_0^e,ξ_1^e in the E population and ξ_0^i,ξ_1^i in the I population (which must be determined and tracked separately), reducing (4) to

$$\begin{aligned} -c\,\partial_\xi V_e + V_e &= \mathcal{W}_e\big(\xi;\,\xi_0^e,\xi_1^e,\xi_0^i,\xi_1^i\big) + I_e(\xi), \\ -c\tau\,\partial_\xi V_i + V_i &= \mathcal{W}_i\big(\xi;\,\xi_0^e,\xi_1^e,\xi_0^i,\xi_1^i\big) + I_i(\xi), \end{aligned} \tag{5}$$

where

$$\begin{aligned} \mathcal{W}_j\big(\xi;\,\xi_0^e,\xi_1^e,\xi_0^i,\xi_1^i\big) = &\big[W_{je}\big(\xi-\xi_0^e\big) - W_{je}\big(\xi-\xi_1^e\big)\big] \\ &- \big[W_{ji}\big(\xi-\xi_0^i\big) - W_{ji}\big(\xi-\xi_1^i\big)\big] \end{aligned} \tag{6}$$

and $W_{jk}(\xi) = \int_0^\xi w_{jk}(\eta)d\eta$ for $j,k \in \{e,i\}$. Based upon the assumptions on w_{jk}, the functions $W_{jk}(\xi)$ are monotonically increasing over $(-\infty,\infty)$. Hence, $W_{jk}(\xi-\xi_0^k) - W_{jk}(\xi-\xi_1^k)$ for $\xi_0^k < \xi_1^k$ is positive, even-symmetric about $\xi = \frac{1}{2}(\xi_0^k + \xi_1^k)$, and monotonically decreasing to 0 as $|x| \to \infty$.

By variation of parameters, a solution of the form $V_e(\xi) = \alpha_e(\xi)e^{\xi/c}$ and $V_i(\xi) = \alpha_i(\xi)e^{\xi/c\tau}$ satisfies (5) if the functions $\alpha_e(\xi)$ and $\alpha_i(\xi)$ satisfy

$$\begin{aligned} -\partial_\xi \alpha_e(\xi) &= \frac{1}{c} e^{-\xi/c} \left[\mathcal{W}_e\left(\xi; \xi_0^e,\xi_1^e,\xi_0^i,\xi_1^i\right) + I_e(\xi) \right], \\ -\partial_\xi \alpha_i(\xi) &= \frac{1}{c\tau} e^{-\xi/c\tau} \left[\mathcal{W}_i\left(\xi; \xi_0^e,\xi_1^e,\xi_0^i,\xi_1^i\right) + I_i(\xi) \right]. \end{aligned} \quad (7)$$

For the case $c > 0$, we integrate over $[\xi,\infty)$ and assume that $\alpha_e(\xi),\alpha_i(\xi) \to 0$ as $\xi \to \infty$ to arrive at

$$\begin{aligned} \alpha_e(\xi) &= \frac{1}{c} \int_\xi^\infty e^{-\eta/c} \left[\mathcal{W}_e(\eta) + I_e(\eta) \right] d\eta, \\ \alpha_i(\xi) &= \frac{1}{c\tau} \int_\xi^\infty e^{-\eta/c\tau} \left[\mathcal{W}_i(\eta) + I_i(\eta) \right] d\eta \end{aligned} \quad (8)$$

and, thereby, obtain the following integral representation for a *traveling bump solution* (V_e,V_i),

$$\begin{aligned} V_e(\xi) &= \frac{1}{c} \int_\xi^\infty e^{(\xi-\eta)/c} \left[\mathcal{W}_e\left(\eta; \xi_0^e,\xi_1^e,\xi_0^i,\xi_1^i\right) + I_e(\eta) \right] d\eta, \\ V_i(\xi) &= \frac{1}{c\tau} \int_\xi^\infty e^{(\xi-\eta)/c\tau} \left[\mathcal{W}_i\left(\eta; \xi_0^e,\xi_1^e,\xi_0^i,\xi_1^i\right) + I_i(\eta) \right] d\eta, \end{aligned} \quad (9)$$

with wave speed c and threshold boundaries $\xi_0^e,\xi_1^e,\xi_0^i,\xi_1^i$. The four unknown values of the five variables $c,\xi_0^e,\xi_1^e,\xi_0^i,\xi_1^i$ of the traveling activity bump (V_e,V_i), depending on the absence or presence of an traveling input, are determined by the set of nonlinear equations

$$V_e\left(\xi_0^e\right) = \theta_e, \quad V_e\left(\xi_1^e\right) = \theta_e, \quad (10)$$

$$V_e\left(\xi_0^i\right) = \theta_i, \quad V_i\left(\xi_1^i\right) = \theta_i, \quad (11)$$

provided such a solution results in a wave profile (V_e,V_i) satisfying threshold conditions (2) and (3) on all of $(-\infty,\infty)$. The traveling bump solution (V_e,V_i) also satisfies (5), so an alternate expression for the traveling bump profile is

$$\begin{aligned} V_e(\xi) &= c\frac{\partial V_e}{\partial \xi}(\xi) + \left[\mathcal{W}_e\left(\xi; \xi_0^e,\xi_1^e,\xi_0^i,\xi_1^i\right) + I_e(\xi) \right], \\ V_i(\xi) &= c\tau\frac{\partial V_i}{\partial \xi}(\xi) + \left[\mathcal{W}_i\left(\xi; \xi_0^e,\xi_1^e,\xi_0^i,\xi_1^i\right) + I_i(\xi) \right], \end{aligned} \quad (12)$$

which contains terms without explicit integrals of $\mathcal{W}_j$.

The ξ *derivative* of the bump can be expressed as

$$\begin{aligned} c\frac{\partial V_e}{\partial \xi}(\xi) &= \int_\xi^\infty e^{(\xi-\eta)/} c \left[\mathcal{W}_e'(\eta) + I_e'(\eta) \right] d\eta, \\ c\tau\frac{\partial V_i}{\partial \xi}(\xi) &= \int_\xi^\infty e^{(\xi-\eta)/} c\tau \left[\mathcal{W}_i'(\eta) + I_i'(\eta) \right] d\eta, \end{aligned} \quad (13)$$

which follows from (9) if $\mathcal{W}_e(\xi),\mathcal{W}_i(\xi)$ and $I_e(\xi),I_i(\xi)$ are continuously differentiable. The ξ derivative plays a role in stability of the bump, and the form (13) is used to calculate the traveling bump profile $(V_e(\xi),V_i(\xi))$ explicitly in Sec. II C using (12) and

$$\mathcal{W}_j'(\xi) = \left[w_{je}\left(\xi - \xi_0^e\right) - w_{je}\left(\xi - \xi_1^e\right) \right] \quad (14)$$

$$-\left[w_{ji}\left(\xi - \xi_0^i\right) - w_{ji}\left(\xi - \xi_1^i\right) \right]. \quad (15)$$

A. Traveling waves with negative wave speeds

For the case $c < 0$, any left-moving traveling bump profile $(V_e(\xi),V_i(\xi))$ is always a reflection (across $\xi = 0$) of some right-moving traveling bump profile, traveling with speed $|c|$. This is seen from the invariance of Eqs. (5) under the transformation

$$\begin{aligned} (c,\xi) &\mapsto (-c,-\xi), \\ \left(\xi_0^e,\xi_1^e,\xi_0^i,\xi_1^i\right) &\mapsto \left(-\xi_1^e,-\xi_0^e,-\xi_1^i,-\xi_0^i\right), \end{aligned}$$

which is due to the following symmetry of $\mathcal{W}_e,\mathcal{W}_i$:

$$\mathcal{W}_j\left(-\xi; -\xi_1^e,-\xi_0^e,-\xi_1^i,-\xi_0^i\right) = \mathcal{W}_j\left(\xi; \xi_0^e,\xi_1^e,\xi_0^i,\xi_1^i\right)$$

(W_{jk} is odd symmetric) and the even symmetry of I_e,I_i. One can also show explicitly that any bump profile with $c < 0$ is a reflection across $\xi = 0$ of a bump profile for the corresponding value $|c| > 0$ working with the case $c < 0$ and keeping track of threshold points $(\xi_{0,1}^e,\xi_{0,1}^i)$.

B. Existence equations and simulations

Traveling wave solutions were examined both (i) by solving the existence equations (10) and (11) numerically for the values $c,\xi_0^e,\xi_1^e,\xi_0^i,\xi_1^i$ and (ii) by evolving the neural field equation in numerical simulations and studying the approach of solutions to stable traveling waves. Estimated values of $c,\xi_0^e,\xi_1^e,\xi_0^i,\xi_1^i$ were also calculated from simulations and compared. All calculations were made with the functions listed in Sec. II C. Whenever stable waves in numerical simulations of (1) were generated, their widths and wave profiles consistently matched those found by numerically solving existence equations (10) and (11). Wave profiles are shown in Fig. 1 as the relative inhibitory time constant varies. The increased delay in the I population allows the leading excitatory activity bump to be more pronounced and the wave propagates faster. Wave speed c increases with increasing τ as does the width of the traveling bump. In Sec. V F, we will return to this parameter regime to investigate the case of $\tau < 1.2$, examining more closely the bifurcation structure that gives rise to these traveling waves as τ is decreased.

C. Explicit calculations of the traveling bump profile and gradient for Gaussian $w_{jk}(\xi)$ and $I(\xi)$

Below we list explicit expressions for a traveling bump profile $(V_e(\xi),V_i(\xi))$ in the case of Gaussian synaptic weight functions of the form

$$w_{jk}(\xi) = \frac{1}{\sqrt{\pi}} \frac{\bar{w}_{jk}}{\sigma_{jk}} e^{-(\xi/\sigma_{jk})^2} \quad (16)$$

and Gaussian input inhomogeneities of the form

$$I_j(\xi) = I_{j\circ} e^{-(\xi/\sigma_j)^2}. \quad (17)$$

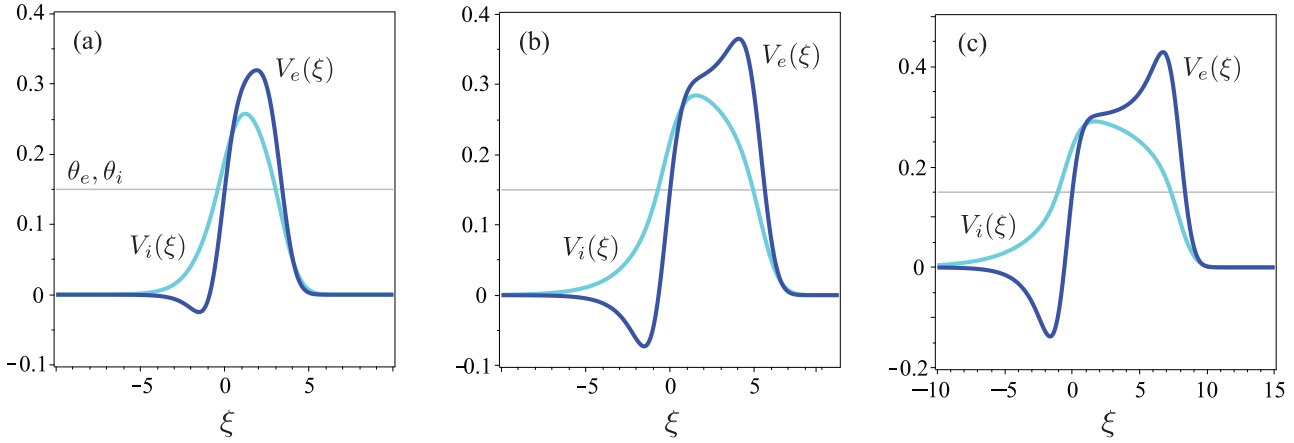

FIG. 1. Traveling bump wave profiles $V_e(\xi), V_i(\xi)$ in traveling wave coordinates for different time constants of inhibition τ. In this parameter regime, as τ increases from (a) $\tau = 1.2$ to (b) $\tau = 1.5$ to (c) $\tau = 2.0$, the wave speed increases from $c = 0.77$ to $c = 1.1$ to $c = 1.3$, accordingly. Waves in this parameter regime are determined to be stable using the Evans function (Sec. III) and numerical simulations. Other parameters are $\bar{w}_{ee} = 1$, $\bar{w}_{ei} = 0.7$, $\bar{w}_{ie} = 0.55$, $\bar{w}_{ii} = 0.24$, $\sigma_{ee} = \sigma_{ei} = \sigma_{ii} = 1$, $\sigma_{ie} = 1.3$, $\theta_e = \theta_i = 0.15$, $I_\circ = 0$.

In particular, we have

$$W_{jk}(\xi) = \int_0^\xi w_{jk}(\eta)d\eta = \frac{\bar{w}_{jk}}{2}\,\mathrm{erf}\left(\frac{\xi}{\sigma_{jk}}\right). \tag{18}$$

We define and express the function $G_{jk}(x,\xi,\rho)$, where $j,k \in \{e,i\}$, $\rho \in \{c, c\tau\}$, $n \in \{0,1\}$, as

$$\begin{aligned} G_{jk}\big(x,\xi_n^k,\rho\big) &= \int_x^\infty e^{(x-\eta)/\rho}\, w_{jk}\big(\eta - \xi_n^k\big)\, d\eta \\ &= \frac{\bar{w}_{jk}}{2} e^{(\sigma_{jk}/2\rho)^2} e^{(x-\xi_n^k/\rho)}\,\mathrm{erfc}\left(\frac{\sigma_{jk}}{2\rho} + \frac{x-\xi_n^k}{\sigma_{jk}}\right) \end{aligned}$$

and the function $J_j(x,\rho)$ where $j \in \{e,i\}$ and $\rho \in \{c, c\tau\}$,

$$\begin{aligned} &J_j(x,\rho) \\ &= \int_x^\infty e^{(x-\eta)/\rho}\, I_j'(\eta)\, d\eta \\ &= I_{j\circ}\left[\frac{\sqrt{\pi}\sigma_j}{2\rho} e^{(\sigma_j/2\rho)^2} e^{x/\rho}\,\mathrm{erfc}\left(\frac{\sigma_j}{2\rho} + \frac{x}{\sigma_j}\right) - e^{-(x/\sigma_j)^2}\right]. \end{aligned}$$

Terms in $\mathcal{W}_j'(\xi)$ are all of the form $w_{jk}(\xi)$ or $I_j'(\xi)$; accordingly, the ξ derivative of the traveling bump is

$$\begin{aligned} c\frac{\partial V_e}{\partial \xi}(\xi) &= \big[G_{ee}\big(\xi,\xi_0^e,c\big) - G_{ee}\big(\xi,\xi_1^e,c\big)\big] \\ &\quad - \big[G_{ei}\big(\xi,\xi_0^i,c\big) - G_{ei}\big(\xi,\xi_1^i,c\big)\big] + J_e(\xi,c), \\ c\tau\frac{\partial V_i}{\partial \xi}(\xi) &= \big[G_{ie}\big(\xi,\xi_0^e,c\tau\big) - G_{ie}\big(\xi,\xi_1^e,c\tau\big)\big] \\ &\quad - \big[G_{ii}\big(\xi,\xi_0^i,c\tau\big) - G_{ii}\big(\xi,\xi_1^i,c\tau\big)\big] + J_i(\xi,c\tau). \end{aligned} \tag{19}$$

The *traveling bump profile* $(V_e(\xi), V_i(\xi))$ can then be expressed explicitly using (12) and (19) together with (6) and (18) which avoids integrals of $\mathcal{W}_j$ explicitly.

III. STABILITY CONDITIONS FOR TRAVELING BUMP SOLUTIONS

Linearizing (1) in traveling wave coordinates about the traveling bump solution $(V_e(\xi), V_i(\xi))^{\mathrm{T}}$, the perturbations $(\tilde{\varphi}_e, \tilde{\varphi}_i)^{\mathrm{T}}$ to first order formally satisfy

$$\begin{aligned} \frac{\partial \tilde{\varphi}_e}{\partial t} - c\frac{\partial \tilde{\varphi}_e}{\partial \xi} + \tilde{\varphi}_e &= \mathcal{N}_{ee}\,\tilde{\varphi}_e - \mathcal{N}_{ei}\,\tilde{\varphi}_i, \\ \tau\frac{\partial \tilde{\varphi}_i}{\partial t} - c\tau\frac{\partial \tilde{\varphi}_i}{\partial \xi} + \tilde{\varphi}_i &= \mathcal{N}_{ie}\,\tilde{\varphi}_e - \mathcal{N}_{ii}\,\tilde{\varphi}_i, \end{aligned} \tag{20}$$

where $\mathcal{N}_{jk}$ is a nonlocal compact linear operator

$$\begin{aligned} \mathcal{N}_{jk}\,\tilde{\varphi}_k &= w_{jk} * \big[\mathrm{H}'(V_k - \theta_k)\,\tilde{\varphi}_k\big] \\ &= \int_{-\infty}^\infty w_{jk}(\xi-\eta)\,\delta\big(V_k(\eta) - \theta_k\big)\,\tilde{\varphi}_k(\eta,t)\,d\eta \\ &= \frac{w_{jk}(\xi-\xi_0^k)}{|V_k'(\xi_0^k)|}\tilde{\varphi}_k(\xi_0^k,t) + \frac{w_{jk}(\xi-\xi_1^k)}{|V_k'(\xi_1^k)|}\tilde{\varphi}_k(\xi_1^k,t). \end{aligned}$$

Setting $(\tilde{\varphi}_e(\xi,t), \tilde{\varphi}_i(\xi,t))^{\mathrm{T}} = (\varphi_e(\xi), \varphi_i(\xi))^{\mathrm{T}} e^{\lambda t}$ in (20) we obtain the spectral problem

$$(\mathbf{L} + \mathbf{N})\begin{pmatrix}\varphi_e \\ \varphi_i\end{pmatrix} = \lambda\begin{pmatrix}\varphi_e \\ \varphi_i\end{pmatrix}, \tag{21}$$

where linear operators $\mathbf{L}$ and $\mathbf{N}$ are defined by

$$\begin{aligned} \mathbf{L} &= c\frac{\partial}{\partial \xi} - \begin{bmatrix}1 & 0 \\ 0 & \frac{1}{\tau}\end{bmatrix}, \\ \mathbf{N}\begin{pmatrix}\varphi_e \\ \varphi_i\end{pmatrix} &= \begin{pmatrix}\mathcal{N}_{ee}\,\varphi_e - \mathcal{N}_{ei}\,\varphi_i \\ \frac{1}{\tau}\mathcal{N}_{ie}\,\varphi_e - \frac{1}{\tau}\mathcal{N}_{ii}\,\varphi_i\end{pmatrix}. \end{aligned}$$

$\mathbf{N}$ is a compact operator. The essential spectra of $(\mathbf{L}+\mathbf{N})$ and $\mathbf{L}$ are the same, since $\mathbf{L}+\mathbf{N}$ is a compact perturbation of $\mathbf{L}$, and comprise the two lines in the complex plane,

$$\lambda = -1 + i\alpha, \quad \lambda = -\frac{1}{\tau} + i\gamma,$$

where $\alpha, \gamma \in \mathbb{R}$. As $\tau > 0$, these lines lie in the open left half complex plane and do not contribute to instability.

Spectral stability of the traveling bump is consequently determined by elements of the point spectrum where $\mathrm{Re}\,\lambda > \max\{-1,-\frac{1}{\tau}\}$. The wave is linearly stable if eigenvalue $\lambda = 0$ associated with translation invariance is simple and no other eigenvalues lie in the closed right half plane. To identify the point spectrum in this region, we derive an Evans function, by constructing a bounded inverse of operator $(\mathbf{L}+\mathbf{N}-\lambda)$ as a solution to

$$(\mathbf{L}+\mathbf{N}-\lambda)\boldsymbol{\varphi} = \boldsymbol{f}, \tag{22}$$

with $\boldsymbol{f} = (f_e, f_i)^{\mathrm{T}}$, to identify where invertibility fails.

Since $\mathbf{N}(\varphi_e,\varphi_i)^{\mathrm{T}}$ involves the nonlocal evaluation of φ_e,φ_i at points $\xi = \xi_0^e,\xi_1^e,\xi_0^e,\xi_1^i$, we treat this as a nonhomogeneous term and use a self-consistency condition with the constructed solution to determine these values. By variation of parameters, solutions $\boldsymbol{\varphi} = (\varphi_e,\varphi_e)^{\mathrm{T}}$ of (22) can be expressed in the form

$$\boldsymbol{\varphi} \;=\; \Phi\begin{pmatrix}\beta_e(\xi)\\ \beta_i(\xi)\end{pmatrix}, \quad \Phi = [\boldsymbol{\phi}_1|\boldsymbol{\phi}_2],$$

where $\boldsymbol{\phi}_1(\xi) = \binom{1}{0}e^{(\lambda+1)\xi/c}$ and $\boldsymbol{\phi}_2(\xi) = \binom{0}{1}e^{(\lambda+\tau^{-1})\xi/c}$ comprise a fundamental set of solutions for $(\mathbf{L}-\lambda)\mathbf{u} = \mathbf{0}$. Consequently, $\binom{\beta_e(\xi)}{\beta_i(\xi)}$ satisfies

$$-c\,\Phi(\xi)\,\frac{\partial}{\partial\xi}\begin{pmatrix}\beta_e\\ \beta_i\end{pmatrix} \;=\; \begin{pmatrix}\mathcal{N}_{ee}\,\varphi_e - \mathcal{N}_{ei}\,\varphi_i - f_e\\ \frac{1}{\tau}\mathcal{N}_{ie}\,\varphi_e - \frac{1}{\tau}\mathcal{N}_{ii}\,\varphi_i - f_i\end{pmatrix}. \tag{23}$$

For $c > 0$, $\mathrm{Re}\,\lambda > \max\{-1,-\frac{1}{\tau}\}$, integrating over $[\xi,\infty)$ and assuming that $\beta_e(\xi),\beta_i(\xi) \to 0$ as $\xi \to \infty$ results in

$$\begin{pmatrix}\beta_e(\xi)\\ \beta_i(\xi)\end{pmatrix} = \begin{pmatrix}\frac{1}{c}\int_\xi^\infty e^{-[(\lambda+1)/c]\eta}[\,\mathcal{N}_{ee}\,\varphi_e - \mathcal{N}_{ei}\,\varphi_i - f_e\,]\,d\eta\\ \frac{1}{c\tau}\int_\xi^\infty e^{-(\lambda/c+1/c\tau)\eta}[\mathcal{N}_{ie}\varphi_e - \mathcal{N}_{ii}\varphi_i - \tau f_i]d\eta\end{pmatrix}.$$

It then follows that $(\varphi_e,\varphi_i)^{\mathrm{T}}$ must satisfy the system of integral equations

$$\begin{aligned}\varphi_e(\xi) &= \frac{1}{c}\int_\xi^\infty e^{[(\lambda+1)/c](\xi-\eta)}[\mathcal{N}_{ee}\,\varphi_e - \mathcal{N}_{ei}\,\varphi_i - f_e]\,d\eta,\\ \varphi_i(\xi) &= \frac{1}{c\tau}\int_\xi^\infty e^{(\lambda/c+1/c\tau)(\xi-\eta)}[\mathcal{N}_{ie}\,\varphi_e - \mathcal{N}_{ii}\,\varphi_i - \tau f_i]\,d\eta.\end{aligned} \tag{24}$$

Next, defining the functions K_{jk} and F_j where

$$\begin{aligned}K_{jk}\big(\xi;\xi_n^k,\rho,\lambda\big) &= \frac{1}{\rho\big|V_k'\big(\xi_n^k\big)\big|}\int_\xi^\infty e^{(\lambda/c+1/\rho)(\xi-\eta)}w_{jk}\big(\eta-\xi_n^k\big)d\eta,\\ F_j(\xi;\rho,\lambda) &= -\frac{1}{c}\int_\xi^\infty e^{(\lambda/c+1/\rho)(\xi-\eta)}\,f_j(\eta)\,d\eta,\end{aligned} \tag{25}$$

where $j,k \in \{e,i\}$, $n \in \{0,1\}$ and defining $\iota_e = 1$ and $\iota_i = -1$, we reexpress (24) as

$$\begin{aligned}\varphi_e(\xi) - \sum_{k\in\{e,i\}}\sum_{n=0}^{1}\iota_k\,K_{ek}\big(\xi;\xi_n^k,c,\lambda\big)\,\varphi_k\big(\xi_n^k\big) &= F_e(\xi,c),\\ \varphi_i(\xi) - \sum_{k\in\{e,i\}}\sum_{n=0}^{1}\iota_k\,K_{ik}\big(\xi;\xi_n^k,c\tau,\lambda\big)\varphi_k\big(\xi_n^k\big) &= F_i(\xi,c\tau).\end{aligned} \tag{26}$$

The unknown values $\varphi_e(\xi_0^e),\varphi_e(\xi_1^e),\varphi_i(\xi_0^i),\varphi_i(\xi_1^i)$ in (26), collected in vector $\boldsymbol{\psi}$ below,

$$\boldsymbol{\psi} = \big(\varphi_e\big(\xi_0^e\big),\varphi_e\big(\xi_1^e\big),\varphi_i\big(\xi_0^i\big),\varphi_i\big(\xi_1^i\big)\big)^{\mathrm{T}},$$

are determined by setting $\xi = \xi_0^j,\xi_1^j$ for $j \in \{e,i\}$ in (26) to obtain a *compatibility condition* on $\boldsymbol{\psi}$ below

$$[I - M(\lambda)]\boldsymbol{\psi} = \mathbf{F}, \tag{27}$$

where $M(\lambda)$ is a 4×4 matrix given by

$$M = \begin{bmatrix}M_{ee} & -M_{ei}\\ M_{ie} & -M_{ii}\end{bmatrix},$$

whose submatrices for $k \in \{e,i\}$ are given by

$$M_{ek} = \begin{bmatrix}K_{ek}\big(\xi_0^e;\xi_0^k,c,\lambda\big) & K_{ek}\big(\xi_0^e;\xi_1^k,c,\lambda\big)\\ K_{ek}\big(\xi_1^e;\xi_0^k,c,\lambda\big) & K_{ek}\big(\xi_1^e;\xi_1^k,c,\lambda\big)\end{bmatrix},$$

$$M_{ik} = \begin{bmatrix}K_{ik}\big(\xi_0^i;\xi_0^k,c\tau,\lambda\big) & K_{ik}\big(\xi_0^i;\xi_1^k,c\tau,\lambda\big)\\ K_{ik}\big(\xi_1^i;\xi_0^k,c\tau,\lambda\big) & K_{ik}\big(\xi_1^i;\xi_1^k,c\tau,\lambda\big)\end{bmatrix},$$

and $\mathbf{F} = (F_e(\xi_0^e,c),F_e(\xi_1^e,c),F_i(\xi_0^i,c\tau),F_i(\xi_1^i,c\tau))^{\mathrm{T}}$.

Compatibility condition (27) gives rise to a unique solution $(\varphi_e,\varphi_i)^{\mathrm{T}}$ whenever λ is such that

$$\mathsf{det}[I - M(\lambda)] \neq 0.$$

In this case, the operator $(\mathbf{L}+\mathbf{N}-\lambda)$ is one-to-one with a continuous inverse that is defined on its range and given by integral representation (24) where $\boldsymbol{\psi}$ satisfies (27). These λ comprise the resolvent set of $(\mathbf{L}+\mathbf{N})$.

$(\mathbf{L}+\mathbf{N}-\lambda)$ is not one-to-one on the set of λ where $\mathrm{Re}\,\lambda > \max\{-1,-\frac{1}{\tau}\}$ when $\mathsf{det}[I - M(\lambda)] = 0$ in which case there exist nontrivial solutions to $(\mathbf{L}+\mathbf{N}-\lambda)\boldsymbol{\varphi} = \mathbf{0}$. Such λ lie in the point spectrum of $(\mathbf{L}+\mathbf{N})$. Therefore, an *Evans function* $\mathcal{E}(\lambda)$ for the traveling bump is

$$\mathcal{E}(\lambda) = \mathsf{det}[I - M(\lambda)] \tag{28}$$

for $c > 0$ and $\mathrm{Re}\,\lambda > \max\{-1,-\frac{1}{\tau}\}$. The *zero set* of the Evans function is the set of all eigenvalues in this region.

A. Stability calculations and simulations

The stability of traveling bump solutions was investigated using the Evans function and numerical simulation. In Sec. III B, the Evans function is calculated explicitly for the case of Gaussian synaptic weight functions and inputs. In all cases examined, the stability properties of traveling waves arising in numerical simulations of neural field (1) were in agreement with the stability properties of the traveling wave according to the point spectrum identified by the Evans function $\mathcal{E}(\lambda)$.

Furthermore, it was possible to destabilize the traveling bump solution in a Hopf bifurcation. An example is shown in Fig. 2 which depicts the graphs of the zero sets of the real and imaginary parts of the Evans function for two different values of $\bar{w}_{ii}$ on either side of the bifurcation point for the parameter values listed. As a result of translation symmetry in the absence of an input, $\lambda = 0$ is always an eigenvalue. When $\bar{w}_{ii} = 0.185$, the traveling bump has a pair of complex conjugate eigenvalues with negative real part close to 0. In this case, an E-I traveling activity-bump-like initial condition, with a spatial offset between the E and I bumps, evolves towards the stable traveling bump solution. Figure 3 shows decaying oscillations in the width of the (excitatory) activity bump as it approaches the constant wave profile of the stable traveling

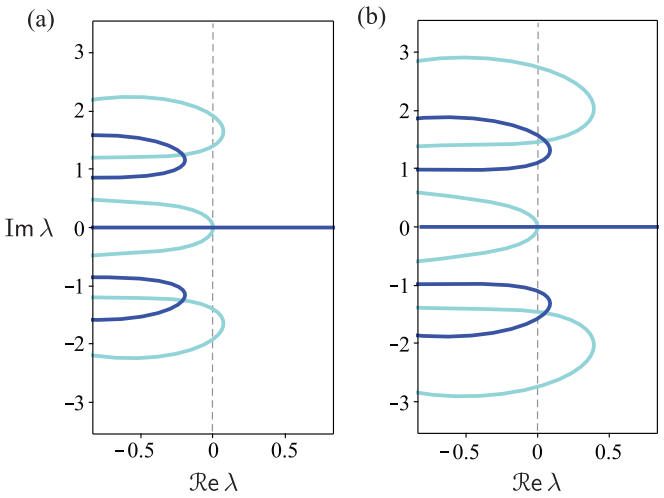

FIG. 2. Graphs of the zero sets of the real (dark) and imaginary (light) parts of the Evans function $\mathcal{E}(\lambda)$ for $\mathrm{Re}\,\lambda > -1/\tau$ in the complex plane where (a) $\bar{w}_{ii} = 0.24$ and (b) $\bar{w}_{ii} = 0.16$. Eigenvalues in the region identify as intersections of the zero sets of the real and imaginary parts of the Evans function. In addition to the persistent 0 eigenvalue, panels (a) and (b) show a pair of complex conjugate eigenvalues crossing the imaginary axis into the open right half plane as $\bar{w}_{ii}$ is decreased, destabilizing the traveling bump in a Hopf bifurcation at $\bar{w}_{ii} \approx 0.172$. Other parameters are as in Fig. 1.

bump. Numerical simulations suggest the Hopf bifurcation is subcritical, with the activity bump collapsing to the rest state (uniform zero solution) when $\bar{w}_{ii}$ is set just beyond the Hopf bifurcation point.

In Sec. V, we further examine the emergence of traveling bump solutions and stable traveling breathers within the larger context of stationary bumps. Initially, we examine a different parameter regime and, subsequently, in Sec. V F, revisit the case of parameters listed in Figs. 1 and 2 for $\tau < 1.2$.

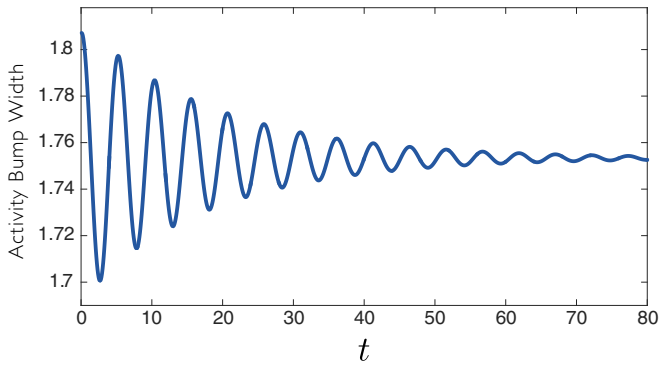

FIG. 3. Graph of the width of a propagating activity bump vs time t (in units of the excitatory time constant) as it evolves towards a stable traveling bump in a simulation of EI neural field (1) for parameters in Fig. 2 with $\bar{w}_{ii} = 0.185$ (only E population shown). At this point, a pair of complex eigenvalues with negative real part is positioned near the imaginary axis. The imaginary part is 1.221 which closely matches the oscillation frequency in the simulation (crest-to-crest time interval length is approximately 5.15). At the bifurcation point $\bar{w}_{ii} \approx 0.172$, the Hopf frequency is $\omega_{\mathcal{H}} = 1.355$.

B. Explicit calculation of the Evans function $\mathcal{E}(\lambda)$ for a traveling bump for a Gaussian $w_{uv}(\xi)$ and $I(\xi)$

In the case of Gaussian $w_{jk}(\xi)$ and $I_j(\xi)$ as in (16) and (17) we can express the functions K_{jk} given in (25) as

$$K_{jk}\big(x;\xi_n^k,\rho,\lambda\big) = \frac{1}{\rho\big|V_k'\big(\xi_n^k\big)\big|}\int_x^\infty e^{(\lambda/c+1/\rho)(x-\eta)} w_{jk}\big(\eta-\xi_n^k\big)d\eta$$
$$= \frac{\overline{w}_{jk}}{2\rho\big|V_k'\big(\xi_n^k\big)\big|}\, e^{(\lambda/c+1/\rho)^2(\sigma_{jk}/2)^2} e^{(\lambda/c+1/\rho)(x-\xi_n^k)}$$
$$\times\ \mathrm{erfc}\left[\frac{\sigma_{jk}}{2}\left(\frac{\lambda}{c}+\frac{1}{\rho}\right)+\frac{x-\xi_n^k}{\sigma_{jk}}\right] \qquad (29)$$

with $V_k'(\xi_n^k)$ for $k \in \{e,i\}$, $n \in \{0,1\}$ calculated in (19). Thus, the Evans function $\mathcal{E}(\lambda)$ for $\mathrm{Re}\,\lambda > \max\{-1,-\frac{1}{\tau}\}$ and $c > 0$ is given by (28) with $K_{jk}(x;\xi_n^k,\rho,\lambda)$ in (29) and with c and $(\xi_0^e,\xi_1^e,\xi_0^i,\xi_1^i)$ determined by (10) and (11).

IV. REDUCTION IN THE LIMIT $c \to 0$: CONDITIONS FOR THE EXISTENCE AND STABILITY OF STATIONARY BUMPS

The existence and stability results for traveling bumps in Secs. II and III reduce, in the limit as speed $c \to 0^+$, to the case of stationary bumps as developed in [23,52]. To show this, we establish the following identity for $\rho > 0$:

$$\lim_{\rho\to 0^+}\frac{1}{\rho}\int_\xi^\infty e^{(\xi-\eta)/\rho} f(\eta)\,d\eta \;=\; f(\xi), \qquad (30)$$

assuming that $f(\xi)$ is continuous and bounded over $\mathbb{R}$.

To prove (30), we recognize that for all $\rho > 0$ and all continuous and bounded f, the function $e^{-\tilde{\eta}} f(\rho\tilde{\eta}+\xi)$ is Lebesgue integrable over $[0,\infty)$ for each fixed $\xi \in \mathbb{R}$. So the following integral converges and can be rewritten as

$$\frac{1}{\rho}\int_\xi^\infty e^{(\xi-\eta)/\rho} f(\eta)\,d\eta \;=\; \int_0^\infty e^{-\tilde{\eta}} f(\rho\tilde{\eta}+\xi)\,d\tilde{\eta}. \qquad (31)$$

From the continuity of f it also follows that

$$\lim_{\rho\to 0^+} f(\rho\tilde{\eta}+\xi) = f(\xi).$$

Then, by the Lebesgue dominated convergence theorem,

$$\lim_{\rho\to 0^+}\frac{1}{\rho}\int_\xi^\infty e^{(\xi-\eta)/\rho} f(\eta)\,d\eta \;=\; \int_0^\infty \lim_{\rho\to 0^+} e^{-\tilde{\eta}} f(\rho\tilde{\eta}+\xi)\,d\tilde{\eta}$$
$$= \int_0^\infty e^{-\tilde{\eta}} f(\xi)\,d\tilde{\eta} = f(\xi).$$

A. Stationary bump: Profile and existence

Let $V_e^\circ(\xi)$ and $V_i^\circ(\xi)$ denote the bump profiles resulting from taking the limit $c \to 0^+$ in (9), i.e.,

$$V_e^\circ(\xi) \equiv \lim_{c\to 0^+} V_e(\xi), \quad V_i^\circ(\xi) \equiv \lim_{c\to 0^+} V_i(\xi).$$

Consequently, applying (30) to (9) we have that

$$V_e^\circ(\xi) = \lim_{c\to 0^+}\frac{1}{c}\int_\xi^\infty e^{(\xi-\eta)/c}\big[\mathcal{W}_e\big(\eta;\,\xi_0^e,\xi_1^e,\xi_0^i,\xi_1^i\big)+I_e(\eta)\big]\,d\eta$$
$$= \mathcal{W}_e\big(\xi;\,\xi_0^e,\xi_1^e,\xi_0^i,\xi_1^i\big)+I_e(\xi). \qquad (32)$$

And, since $\tau > 0$, then $\rho = c\tau \longrightarrow 0^+$ as $c \to 0^+$ so that

$$V_i^\circ(\xi) = \lim_{\rho\to 0^+} \frac{1}{\rho}\int_\xi^\infty e^{(\xi-\eta)/\rho}\left[\mathcal{W}_i\left(\eta;\xi_0^e,\xi_1^e,\xi_0^i,\xi_1^i\right)+I_i(\eta)\right]d\eta$$
$$= \mathcal{W}_i\left(\xi;\,\xi_0^e,\xi_1^e,\xi_0^i,\xi_1^i\right) + I_i(\xi). \tag{33}$$

Equations (32) and (33) match the stationary bump profiles in E and I populations developed for the stationary bump case in [23,52] assuming, by translation symmetry, that the bump (and localized input, when present) is centered about the origin and threshold boundaries are accordingly taken to be $(\xi_0^e,\xi_1^e,\xi_0^i,\xi_1^i) = (-\xi_e,\xi_e,-\xi_i,\xi_i)$.

The existence conditions for a stationary bump,

$$V_e^\circ(\pm\xi_e) = \theta_e, \quad V_i^\circ(\pm\xi_i) = \theta_i,$$

naturally follow as they are based upon the stationary bump profiles (32) and (33). Analogously, from (13) we have the following limiting result for the gradient of the stationary bump (which is relevant for stability):

$$\frac{\partial V_e^\circ}{\partial\xi}(\xi) \equiv \lim_{c\to 0^+}\frac{\partial V_e}{\partial\xi}(\xi) = \mathcal{W}_e'\left(\xi;\,\xi_0^e,\xi_1^e,\xi_0^i,\xi_1^i\right)+I_e'(\xi),$$
$$\frac{\partial V_i^\circ}{\partial\xi}(\xi) \equiv \lim_{\rho\to 0^+}\frac{\partial V_i}{\partial\xi}(\xi) = \mathcal{W}_i'\left(\xi;\,\xi_0^e,\xi_1^e,\xi_0^i,\xi_1^i\right)+I_i'(\xi), \tag{34}$$

where $\mathcal{W}_j'$ is given in (15).

B. Stationary bump stability and Evans function

Analogous to Sec. IV A, we examine the Evans function $\mathcal{E}(\lambda)$ given in (28) in the limit as speed $c \longrightarrow 0^+$. The matrix elements of the Evans function $\mathcal{E}(\lambda)$ in (28) are expressed in terms of functions $K_{jk}(\xi;\xi_n^k,\rho,\lambda)$ for $\mathrm{Re}\,\lambda > \max\{-1,-\frac{1}{\tau}\}$ which can be rewritten as

$$K_{jk}\left(\xi;\xi_n^k,\rho,\lambda\right)$$
$$= \frac{1}{\rho\left|V_k'\left(\xi_n^k\right)\right|}\int_\xi^\infty e^{(\lambda/c+1/\rho)(\xi-\eta)}w_{jk}\left(\eta-\xi_n^k\right)d\eta$$
$$= \frac{1}{\rho\left(\frac{\lambda}{c}+\frac{1}{\rho}\right)}\frac{1}{\left|V_k'\left(\xi_n^k\right)\right|}\int_0^\infty e^{-\tilde\eta}\,w_{jk}\left(\tfrac{\tilde\eta}{\frac{\lambda}{c}+\frac{1}{\rho}}+\xi-\xi_n^k\right)d\eta.$$

Applying identity (30) to $K_{jk}(\xi;\xi_n^k,\rho,\lambda)$, for the case $j = e$ where $\rho = c$, results in

$$K_{ek}^\circ\left(\xi;\xi_n^k,\lambda\right) \equiv \lim_{c\to 0^+} K_{ek}\left(\xi;\xi_n^k,c,\lambda\right)$$
$$= \frac{1}{(\lambda+1)}\frac{1}{\left|V_k'\left(\xi_n^k\right)\right|}\,w_{ek}\left(\xi-\xi_n^k\right)$$

and, for case $j = i$ where $\rho = c\tau$, we similarly have

$$K_{ik}^\circ\left(\xi;\xi_n^k,\lambda\right) \equiv \lim_{c\to 0^+} K_{ik}\left(\xi;\xi_n^k,c\tau,\lambda\right)$$
$$= \frac{1}{\left(\lambda+\frac{1}{\tau}\right)}\frac{1}{\tau\left|V_k'\left(\xi_n^k\right)\right|}\,w_{ik}\left(\xi-\xi_n^k\right).$$

Defining the functions

$$\alpha(\xi) = \frac{w_{ee}(\xi)}{\left|\frac{\partial}{\partial\xi}V_e^\circ(\xi_e)\right|}, \quad \beta(\xi) = -\frac{w_{ei}(\xi)}{\left|\frac{\partial}{\partial\xi}V_i^\circ(\xi_i)\right|},$$
$$\gamma(\xi) = \frac{w_{ie}(\xi)}{\tau\left|\frac{\partial}{\partial\xi}V_e^\circ(\xi_e)\right|}, \quad \delta(\xi) = -\frac{w_{ii}(\xi)}{\tau\left|\frac{\partial}{\partial\xi}V_i^\circ(\xi_i)\right|},$$

where $\xi_{0,1}^e = \pm\xi_e$, $\xi_{0,1}^i = \pm\xi_i$ as discussed in Sec. IV A, and defining the matrix

$$M^\circ = \begin{bmatrix} \alpha(0) & \alpha(2\xi_e) & \beta(\xi_e-\xi_i) & \beta(\xi_e+\xi_i) \\ \alpha(2\xi_e) & \alpha(0) & \beta(\xi_e+\xi_i) & \beta(\xi_e-\xi_i) \\ \gamma(\xi_e-\xi_i) & \gamma(\xi_e+\xi_i) & \delta(0) & \delta(2\xi_i) \\ \gamma(\xi_e+\xi_i) & \gamma(\xi_e-\xi_i) & \delta(2\xi_i) & \delta(0) \end{bmatrix},$$

then for $\mathrm{Re}\,\lambda > \max\{-1,-\frac{1}{\tau}\}$ it can be shown that in the limit as the wave speed $c \to 0$, the Evans function for the stationary ($c = 0$) bump becomes

$$\mathcal{E}^\circ(\lambda) \equiv \lim_{c\to 0^+}\mathcal{E}(\lambda)$$
$$= \frac{1}{(\lambda+1)\left(\lambda+\frac{1}{\tau}\right)}\,\mathrm{det}(D-M^\circ),$$

where

$$D = \mathrm{diag}\left(\lambda+1,\lambda+1,\lambda+\tfrac{1}{\tau},\lambda+\tfrac{1}{\tau}\right).$$

The condition $\mathcal{E}^\circ(\lambda) = 0$ is equivalent to the equation derived in both [23,52] which determines the eigenvalues in the case ($c = 0$) analyzed by assuming the form of a stationary bump rather the traveling bump analyzed herein. For $\mathrm{Re}\,\lambda > \max\{-1,-\tau^{-1}\}$, eigenvalues form the zero set of the function $\mathcal{E}^\circ(\lambda)$ thus reflecting an Evans function. Recall that the set of λ with $\mathrm{Re}\,\lambda = -1$ or $-\tau^{-1}$ comprises the essential spectrum. This analysis moreover determines stability conditions for stationary bumps used in two contexts in this paper: (1) when considering a drift bifurcation from a stationary to a traveling bump as discussed in Sec. V A, and (2) in conjunction with results in Sec. V on stationary and traveling bumps.

V. BIFURCATIONS AND SIMULATIONS: STATIONARY AND TRAVELING BUMPS AND BREATHERS IN AN E-I NEURAL FIELD

A. Drift bifurcation of a stationary bump to a traveling bump in the case of no input ($I_{e,i} = 0$)

In the case of no input inhomogeneity ($I_{e,i} = 0$), a stable traveling bump solution can emerge when a stationary bump undergoes a drift bifurcation, i.e., a pitchfork bifurcation occurring with respect to the translation mode of the linearization in addition to the persistent zero eigenvalue associated with translation symmetry. As developed in [52], and analogous to [50], the linearized operator about the stationary bump contains two spatial two-dimensional eigenmodes whose spatial structure is distinguished by even and odd symmetries. Let $\lambda_\pm^\oplus$ be the eigenvalues associated with the symmetric mode, and $\lambda_\pm^\ominus$ be those associated with the odd-symmetric mode. The odd-symmetric mode (difference mode) forms the translation mode of the system. Generically, $\lambda_+^\ominus = 0$ is a persistent 0 eigenvalue when no input inhomogeneity ($I_{e,i} = 0$) is present, reflecting the translational symmetry of the network. As a consequence, it can be shown that the other eigenvalue in the difference mode is

$$\lambda_-^\ominus = -1 - \frac{1}{\tau} + \frac{w_{ee}(0)-w_{ee}(2\xi_e)}{\Gamma_e} - \frac{w_{ii}(0)-w_{ii}(2\xi_i)}{\tau\Gamma_i},$$

where Γ_e, $\Gamma_i > 0$, and

$$\Gamma_e = [w_{ee}(0) - w_{ee}(2\xi_e)] - [w_{ei}(\xi_e - \xi_i) - w_{ei}(\xi_e + \xi_i)],$$
$$\Gamma_i = [w_{ie}(\xi_i - \xi_e) - w_{ie}(\xi_i + \xi_e)] - [w_{ii}(0) - w_{ii}(2\xi_i)],$$

as shown in [52] (see also [23]).

A drift bifurcation is expected to occur when the nonidentically zero eigenvalue $\lambda_-^{\ominus}$ associated with the odd-symmetric mode increases through 0 while the other pair of eigenvalues $\lambda_\pm^{\oplus}$ remain in the open left half plane. Any parameter that changes the stationary bump widths ξ_e,ξ_i generically changes this eigenvalue since it depends explicitly on ξ_e,ξ_i. There are various ways $\lambda_-^{\ominus}$ may be increased through 0, thereby destabilizing the stationary bump in a drift bifurcation; two particular ways, examined herein, are by varying the time constant τ and the I-to-I synaptic strength $\bar{w}_{ii}$ The time constant τ is different from other parameters in that it does not determine the *stationary* bump widths ξ_e,ξ_i, only its stability (naturally it does affect the width of a *traveling* bump). Thus, since $\xi_{e,i}$ do not change as τ changes, and since $w_{ii}(0) - w_{ii}(2\xi_i) > 0$ and $\Gamma_i > 0$, an increase in τ necessarily causes eigenvalue $\lambda_-^{\ominus}$ to increase due to the resulting decrease in the magnitude of the negative terms,

$$-\frac{1}{\tau} - \frac{w_{ii}(0) - w_{ii}(2\xi_i)}{\tau\Gamma_i}. \tag{35}$$

Consequently, it is possible for stable stationary bumps to destabilize in a drift bifurcation as τ is increased.

The equation $\lambda_-^{\ominus} = 0$, can be solved for τ to find the corresponding value of $\tau > 0$ to be

$$\tau_{\text{crit}}^{\mathcal{D}} = \frac{1 + \frac{w_{ii}(0) - w_{ii}(2\xi_i)}{\Gamma_i}}{-1 + \frac{w_{ee}(0) - w_{ee}(2\xi_e)}{\Gamma_e}}.$$

Note that $\tau_{\text{crit}}^{\mathcal{D}} > 0$ whenever $w_{ee}(0) - w_{ee}(2\xi_e) > \Gamma_e$ which is always the case since

$$w_{ei}(\xi_e - \xi_i) - w_{ei}(\xi_e + \xi_i) > 0.$$

Alternatively, a reduction in the I-to-I connection strength $\bar{w}_{ii}$ may increase $\lambda_-^{\ominus}$ by reducing the I-to-I term in (35) depending on the magnitude of changes in Γ_i and the excitatory term which depend on ξ_e and ξ_i.

B. Curves of drift and Hopf bifurcations of *stationary* bumps

To explore the transition from stationary to traveling bumps in simulations of the E-I neural field, a *curve of drift bifurcations* of stationary bumps was calculated in a particular region of parameter space (listed in Fig. 4). This was done by assuming an even-symmetric stationary bump profile, solving the corresponding existence equations [where $V_{e,i}$ are given in (32) and (33)]

$$V_e^{\circ}(\xi_e) = \theta_e \qquad V_i^{\circ}(\xi_i) = \theta_i$$

for the stationary bump half widths $\xi_{e,i}$, and simultaneously requiring the conditions for a drift bifurcation of a stationary bump to be met while τ and $\bar{w}_{ii}$ were varied. This curve of drift bifurcations is labeled $\mathcal{D}^{\ominus}$ in Fig. 4.

Hopf instabilities occur in the E-I neural field and a *curve of Hopf bifurcations* of stationary bumps (even-symmetric mode), denoted by $\mathcal{H}^{\oplus}$ in Fig. 4, was similarly plotted by varying the parameters τ and $\bar{w}_{ii}$ in the same parameter regime. Analogous to the case of drift bifurcations, it can be shown that, under the condition that the eigenvalues $\lambda_\pm^{\oplus}$ associated with the even-symmetric mode are complex (see [52]), the critical value of τ corresponding to a Hopf bifurcation is given by

$$\tau_{\text{crit}}^{\mathcal{H}} = \frac{1 + \frac{w_{ii}(0) + w_{ii}(2\xi_i)}{\Gamma_i}}{-1 + \frac{w_{ee}(0) + w_{ee}(2\xi_e)}{\Gamma_e}}.$$

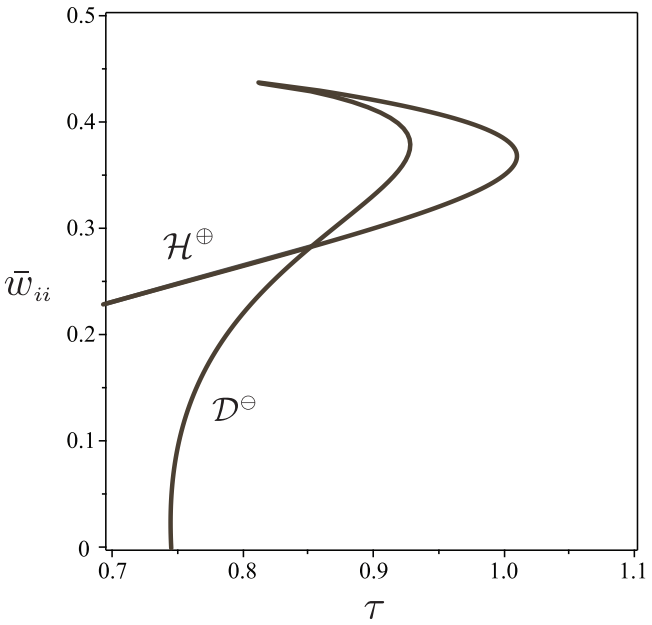

FIG. 4. A curve of drift bifurcations of stationary bumps, denoted by $\mathcal{D}^{\ominus}$, and a curve of Hopf bifurcations of stationary bumps, denoted by $\mathcal{H}^{\oplus}$, in the $\tau\bar{w}_{ii}$ plane. Other (fixed) parameters are $\bar{w}_{ee}=1$, $\bar{w}_{ei}=0.84$, $\bar{w}_{ie}=0.8$, $\sigma_{ee}=\sigma_{ei}=\sigma_{ii}=1$, $\sigma_{ie}=1.3$, $\theta_e=0.16$, $\theta_i=0.24$, $I_{e\circ}=I_{i\circ}=0$.

In Fig. 5, the curves of drift ($\mathcal{D}^{\ominus}$) and Hopf ($\mathcal{H}^{\oplus}$) bifurcations are subdivided into branches $\mathcal{D}_\pm^{\ominus}$ and $\mathcal{H}_\pm^{\oplus}$, respectively, wherein the symbols $-$ $(+)$ denote the branch of each curve along which the opposite spatial eigenmode has eigenvalues with negative (positive) real part. In particular, stationary bumps are stable in region I.

Stationary bumps in region I destabilize in a drift bifurcation across curve $\mathcal{D}_-^{\ominus}$ into region IIa. The traveling wave existence equations were solved numerically in the immediate vicinity of $\mathcal{D}_-^{\ominus}$. Traveling bump solutions were found only in region IIa and not in region I. Wave speed c increased (from speed 0) with distance from curve $\mathcal{D}_-^{\ominus}$ into region IIa. In the immediate vicinity along $\mathcal{D}_-^{\ominus}$ in region IIa, traveling bumps were determined to be stable according to the Evans function. This suggests that the drift bifurcation is supercritical along curve $\mathcal{D}_-^{\ominus}$. Extending beyond, stable traveling waves exist in a large region formed by allowing τ to increase from curve $\mathcal{D}_-^{\ominus}$. Hopf bifurcations of traveling bumps were encountered as reflected by the Evans function. Curves of Hopf bifurcations of *traveling* bumps are calculated in Sec. V C and plotted for the parameter regime listed in Fig. 6. Numerical simulations are investigated further in Sec. V D.

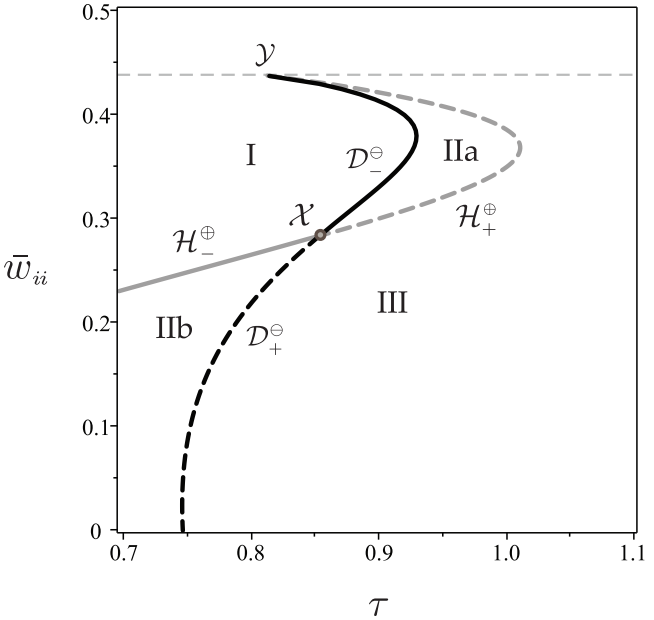

FIG. 5. Subbranches of curves of drift ($\mathcal{D}_{\pm}^{\ominus}$) and Hopf ($\mathcal{H}_{\pm}^{\oplus}$) bifurcations of stationary bumps. Subscripts $_-$ ($_+$) denote where the opposite spatial eigenmode has eigenvalues with negative (positive) real part. Roman numerals denote regions: region I: Re $\lambda_{\pm}^{\oplus}, \lambda_{-}^{\ominus} < 0$; region IIa: $\lambda_{-}^{\ominus} > 0$, Re $\lambda_{\pm}^{\oplus} < 0$; region IIb: Re $\lambda_{\pm}^{\oplus} > 0, \lambda_{-}^{\ominus} < 0$; region III: Re $\lambda_{\pm}^{\oplus}, \lambda_{-}^{\ominus} > 0$.

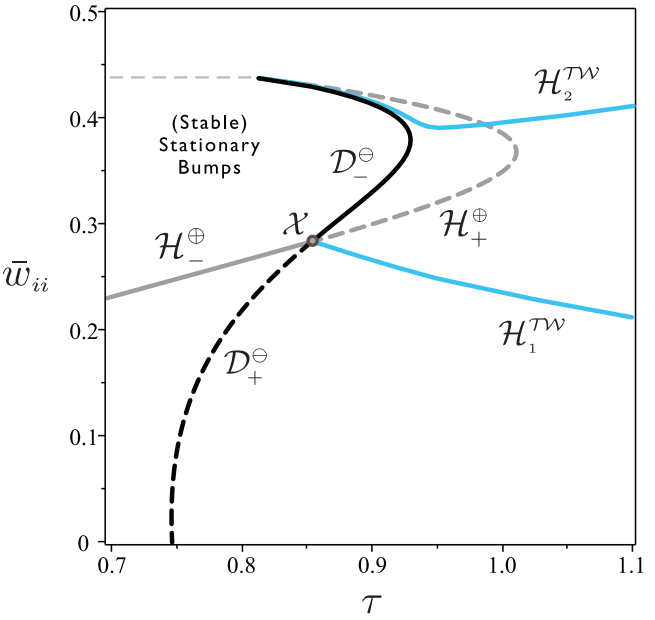

FIG. 6. Curves of Hopf bifurcations $\mathcal{H}_{1,2}^{\mathcal{TW}}$ of traveling bumps indicated in blue. Other curves as described in Fig. 5.

Alternatively, stable stationary bumps in region I destabilize in a Hopf bifurcation (even-symmetric mode) across curve $\mathcal{H}_-^{\oplus}$ into region IIb. Numerical simulations in the vicinity of curve $\mathcal{H}_-^{\oplus}$ in regions I and region IIb are consistent with a supercritical Hopf bifurcation giving rise to stable stationary breathers when crossing $\mathcal{H}_-^{\oplus}$. Numerical simulations in this region and the stable attractors are further discussed in Sec. V D.

Traveling bumps were additionally examined in the vicinity of curve $\mathcal{D}_+^{\ominus}$ of drift bifurcations in Fig. 5 by numerically solving the existence equations and were found only in region III and not in region IIb. Wave speed c increased (from speed 0) from curve $\mathcal{D}_+^{\ominus}$ into region III. These solutions were determined to be unstable according to the Evans function, having a pair of complex eigenvalues with positive real part, which reflects the same structure as the stationary bump undergoing the bifurcation.

Finally, curves $\mathcal{D}_-^{\ominus}$ and $\mathcal{H}_+^{\oplus}$ of drift and Hopf bifurcations of stationary bumps converge at point $\mathcal{Y}$ in Fig. 5. A close examination and analysis of solutions for $\bar{w}_{ii}$ near the level of $\mathcal{Y}$ suggests that the stationary bump widths $\xi_{e,i} \to \infty$ in a narrow interval as $\bar{w}_{ii}$ increases to the level of $\mathcal{Y}$. (This is denoted by the dashed gray line.) Note that $w_{jj}(\xi_j) \to 0$ as $\xi_j \to \infty$ for $j \in \{e,i\}$ which means that $\tau_{\text{crit}}^{\mathcal{H}} \to \tau_{\text{crit}}^{\mathcal{D}}$; thus these curves converge at $\mathcal{Y}$.

C. Curves of Hopf bifurcations of *traveling* bumps

Hopf bifurcations of traveling waves were found to occur in regions IIa and III and were identified using both the Evans function and numerical simulation. In the parameter regime indicated in Fig. 4, two curves of Hopf bifurcations were found to exist and were calculated by numerical continuation from an initial point on each curve, by simultaneously requiring the conditions for the existence of a traveling wave (10) and (11) and a Hopf bifurcation to be met. These curves are plotted and labeled as $\mathcal{H}_{1,2}^{\mathcal{TW}}$ in Fig. 6 and serve as the boundaries of the region of stable traveling waves which lies in between.

Curve $\mathcal{H}_1^{\mathcal{TW}}$ was continued to the immediate vicinity of intersection point $\mathcal{X}$ of the curves of $\mathcal{D}^{\ominus}$ and $\mathcal{H}^{\oplus}$ of drift and Hopf bifurcations of stationary bumps where it became difficult to continue closer to $\mathcal{X}$, possibly due to sensitivity (terms with c^{-1}) arising from the wave speed c tending to zero along this curve as plotted in Fig. 7. As wave speed $c \to 0$, curve $\mathcal{H}_1^{\mathcal{TW}}$ of Hopf bifurcations of traveling bumps should coincide with the intersection of $\mathcal{D}^{\ominus}$ and $\mathcal{H}^{\oplus}$ since the conditions of drift and Hopf bifurcations of a stationary bump are met simultaneously.

The properties (e.g., wave speed, bump widths, spatial offset) of the *stable* traveling waves in the immediate vicinity of the curve of Hopf bifurcations were compared between the solutions of the existence equations (10) and (11) and

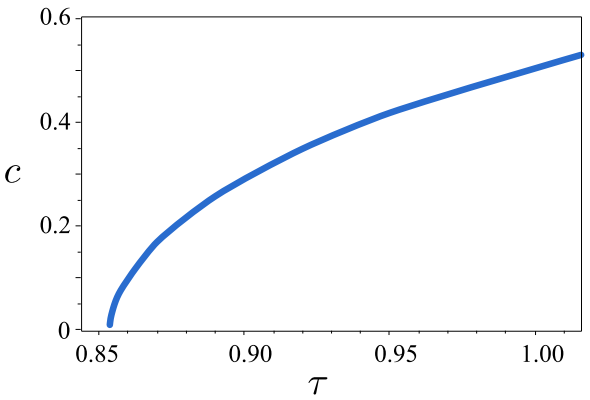

FIG. 7. Wave speed c vs τ along curve $\mathcal{H}_1^{\mathcal{TW}}$.

numerical simulations; these were found to match consistently. Continuing the traveling wave speed, bump widths, and offset of traveling bumps from sampling the existence equations along curves in the region in Fig. 6, it was found that the traveling bumps that destabilize in a Hopf bifurcation traversing curve $\mathcal{H}_1^{\mathcal{TW}}$ continue as the same unstable traveling bumps that bifurcate from drift bifurcations along curve $\mathcal{D}_+^{\ominus}$ (discussed in Sec. V B).

D. Neural field simulations in the vicinity of the curves of drift and Hopf bifurcation in Fig. 6

Numerical simulations of neural field (1) with Gaussian weight functions and no input ($I_{j\circ} = 0$) were used to study the stable attracting solutions in the regions delineated by the curves of drift ($\mathcal{D}_-^{\ominus}$) and Hopf ($\mathcal{H}_-^{\oplus}$) bifurcations of stationary bumps and Hopf bifurcations ($\mathcal{H}_{1,2}^{\mathcal{TW}}$) of traveling bumps plotted in Fig. 6 for the parameter region listed in Fig. 4. The stable attractors, illustrated in Fig. 8, fall into four solution types: stationary bumps, traveling bumps, stationary breathers, traveling breathers.

Initial conditions were taken to be localized activity bumps in both the E and I populations that were either centered around the same point (*syntopic*) or positioned with some spatial offset between centers (*allotopic*). This was chosen with the interest of (1) studying the approach to both stationary and propagating stable activity bumps and to identify any bistability that might exist, (2) examining the dynamics associated with the different eigenmodes of the linearization about a stationary bump, and (3) investigating the super- or subcritical nature of the bifurcations present in a region of parameter space.

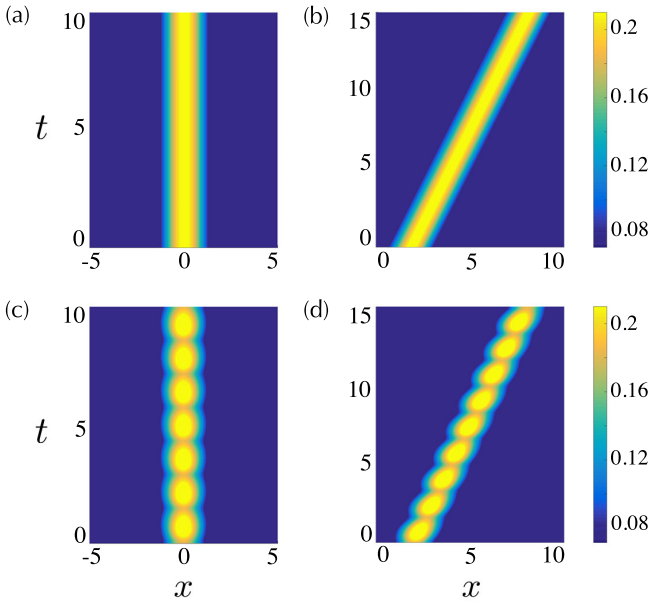

FIG. 8. Space-time plots of $u_e(x,t)$ illustrating the four solution types: (a) stationary bump, (b) traveling bump, (c) stationary breather, (d) traveling breather; [$u_i(x,t)$ not shown]. Parameter values are those listed in Fig. 4 and (a) $(\tau,\bar{w}_{ii}) = (0.84,0.31)$, (b) $(\tau,\bar{w}_{ii}) = (0.96,0.28)$, (c) $(\tau,\bar{w}_{ii}) = (0.83,0.265)$, (d) $(\tau,\bar{w}_{ii}) = (0.96,0.243)$ which are points encircling point $\mathcal{X}$ in the $(\tau,\bar{w}_{ii})$ plane in Fig. 9(b).

Two different types of behavior are found in numerical simulations in the vicinity of the curve $\mathcal{D}_-^{\ominus}$. Recall, in Sec. V B, that curve $\mathcal{D}_-^{\ominus}$ was determined to be a curve of supercritical drift bifurcations according to the existence equations and Evans function. In agreement with this, along the lower section of the curves (roughly $0.29 < \bar{w}_{ii} < 0.39$), numerical simulations, evolving from the offset E-I bump (allotopic) initial conditions, approach a stationary bump for parameter values immediately to the left of $\mathcal{D}_-^{\ominus}$ (in region I) and approached a traveling bump immediately to the right of $\mathcal{D}_-^{\ominus}$ (in region IIa) with the wave speed increasing from speed 0 as τ increased. This gives rise to a large region of stable traveling bump solutions for increasing τ and within a range of $\bar{w}_{ii}$ shaded in blue in Fig. 9(b). And the results of numerical simulations of E-I neural field (1) are in agreement with the existence and stability results using existence equations (10) and (11) and Evans function (28).

The region (blue) of stable traveling bumps is primarily bordered *above* by curve $\mathcal{H}_2^{\mathcal{TW}}$ of Hopf bifurcations of traveling bumps. The Hopf bifurcations on $\mathcal{H}_2^{\mathcal{TW}}$ are supercritical along the branch for (approximately) $\tau > 0.94$. In this case, traveling breathers emerge on the upper side of $\mathcal{H}_2^{\mathcal{TW}}$ with the oscillation amplitude increasing from zero. This region of stable traveling breathers is shaded in green above $\mathcal{H}_2^{\mathcal{TW}}$ in Fig. 9(b). Accordingly, the following sequence of bifurcations, illustrated in Fig. 10, can then be seen along line ℓ_1 as τ increases: a stable stationary bump undergoes a supercritical drift bifurcation to a stable traveling bump which, subsequently, undergoes a supercritical Hopf bifurcation to a stable traveling breather. Conversely, along the branch of $\mathcal{H}_2^{\mathcal{TW}}$ for (approximately) $\tau < 0.94$ beginning from a point near the sharp turn in the curve, the Hopf bifurcation appears to switch to subcritical as suggested by the presence of large-amplitude traveling breathers existing on both sides of $\mathcal{H}_2^{\mathcal{TW}}$ in simulations. For τ approximately in the range $0.915 < \tau < 0.94$, there is a bistable region, indicated by the dark purple region in Fig. 9, where stable traveling bumps and stable traveling breathers both coexist. The following sequence of bifurcations, illustrated in Fig. 10, can then be seen along curve ℓ_2 as τ increases: a stable stationary bump undergoes a supercritical drift bifurcation to a stable traveling bump; at a critical point, a saddle-node bifurcation of limit cycles produces a stable-unstable pair of traveling breathers; at another critical point, the unstable traveling breather coalesces with the stable traveling bump in a subcritical Hopf bifurcation at the intersection with curve $\mathcal{H}_2^{\mathcal{TW}}$; the stable traveling breather and unstable traveling bump continue into the green-shaded region. Alongside, for τ approximately in the range $0.8 < \tau < 0.915$, the region of stable traveling breathers extends farther and overlaps with the region of stable stationary bumps, thereby forming two regions of bistability shown in Fig. 9: (i) the region shaded in light purple, where stable stationary bumps and traveling breathers coexist, and (ii) the region shaded in dark purple, where stable traveling bumps and breathers coexist. A sequence of bifurcations similar to ℓ_2 can then be seen along curve ℓ_3 in Fig. 10 whereupon now the saddle-node bifurcation of limit cycles that produces a stable-unstable pair of traveling breathers instead occurs at a critical point before the drift bifurcation (i.e., to the left of curve $\mathcal{H}_2^{\mathcal{TW}}$) where stationary bumps are stable, with the stationary

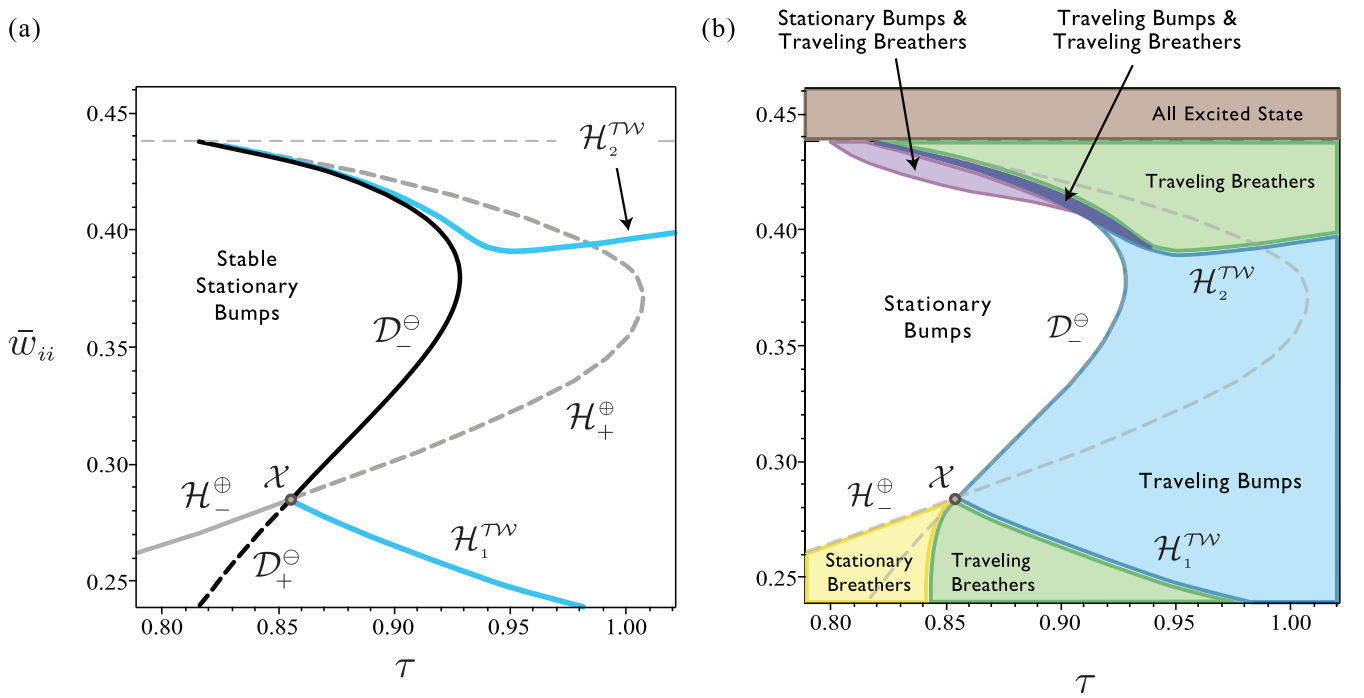

FIG. 9. Bifurcation and simulation results: (a) Curves of drift ($\mathcal{D}_-^{\ominus}$) and Hopf ($\mathcal{H}_-^{\oplus}$) bifurcations of stationary bumps and the curves of Hopf bifurcations ($\mathcal{H}_{1,2}^{TW}$) of traveling bumps in a subregion of the $\tau\bar{w}_{ii}$ plane (depicted in Fig. 6) that was studied extensively in numerical simulations of E-I neural field (1). (b) Different regions indicate the stable attractors that occur in numerical simulations evolving from the offset (allotopic) and centered (syntopic) activity bump initial conditions.

bump continuing through the same sequence of bifurcations as ℓ_2 thereafter. We note that, in the upper part of the green region of traveling breathers above $\mathcal{H}_2^{TW}$, the oscillation amplitude grows with a flare-up type of behavior as $\bar{w}_{ii}$ is increased (since the inhibition becomes less able to control the excitation) until there is a rapid transition that leads to outward propagating fronts approaching the all excited state. The lower boundary of this region corresponds to the level of $\bar{w}_{ii}$ where the stationary bump widths $\xi_{e,i} \to \infty$ rapidly.

The region (blue) of stable traveling bumps in Fig. 9 is bordered *below* by curve $\mathcal{H}_1^{TW}$ of Hopf bifurcations of traveling bumps. We shall now describe a sequence of transitions in the attractor (ω-limit set) of the allotopic bump initial condition that are exhibited in numerical simulations while circumnavigating the point $\mathcal{X}$ at the intersection of curves $\mathcal{D}_-^{\ominus}$, $\mathcal{H}_-^{\oplus}$, and $\mathcal{H}_1^{TW}$. We mention here that both syntopic and allotopic initial conditions were examined and no region of bistability with stationary and traveling bumps or breathers was found to exist in this region. As discussed previously, traversing $\mathcal{D}_-^{\ominus}$, a stable bump undergoes a supercritical drift bifurcation to a stable traveling bump, indicated both in numerical simulations and by the existence equations and Evans function. Traversing $\mathcal{H}_1^{TW}$, a stable traveling bump undergoes a supercritical Hopf bifurcation to a stable traveling breather that forms the attractor in the green region in Fig. 9(b). Continuing further to the left in the $\tau\bar{w}_{ii}$ plane by decreasing τ, numerical simulations show a steady transition from a stable *traveling* breather to a stable *stationary* breather with a graded decrease to speed 0 that occurs when crossing the border from the green region into the yellow region in Fig. 9(b). In the yellow region, a stationary breather forms the stable attractor. This region is bounded on the left by $\mathcal{H}_-^{\oplus}$ which is a curve of Hopf bifurcations that simulations suggest are supercritical bifurcations. Finally, crossing $\mathcal{H}_-^{\oplus}$ into the white region, a stationary bump forms the stable attractor, thereby completing the circumnavigation of $\mathcal{X}$. Note that, at the lower edge in Fig. 9(b) and below, both stationary and traveling breathers become increasingly more difficult to approach in numerical simulations, with the oscillations leading to a collapse of the activity bump to the rest state.

We have concentrated on stable attractors, but, by solving the existence equations, we may also continue the stable traveling bumps that destabilize when traversing $\mathcal{H}_1^{TW}$ as unstable traveling bumps. The wave speed of these unstable traveling bumps decreases to 0 when approaching curve $\mathcal{D}_+^{\ominus}$ of drift bifurcations of (unstable) stationary bumps in Fig. 6, indicating that the *unstable* traveling bump merges with a *unstable* stationary bump in a supercritical drift bifurcation ($\mathrm{Re}\,\lambda_{\pm}^{\oplus} > 0$).

Combining (i) existence and stability results of stationary bumps across $\mathcal{D}_-^{\ominus}$ and $\mathcal{H}_-^{\oplus}$, (ii) the existence and stability results of traveling bumps across $\mathcal{D}_-^{\ominus}$ and $\mathcal{H}_1^{TW}$, in conjunction with (iii) numerical simulations suggests a codimension-2 bifurcation we discuss in Sec. V E, illustrated in Fig. 11.

E. Codimension-2 bifurcation

The results discussed in lower Fig. 9 are suggestive of a codimension-2 bifurcation, which we shall refer to as a *drift-Hopf bifurcation*, with a mode interaction occurring between the odd-symmetric $\lambda_{\pm}^{\ominus}$ eigenmode undergoing a drift instability and the even-symmetric $\lambda_{\pm}^{\oplus}$ eigenmode undergoing a Hopf instability. The codimension-2 point $\mathcal{X}$ forms an organizing center for the dynamics associated with the

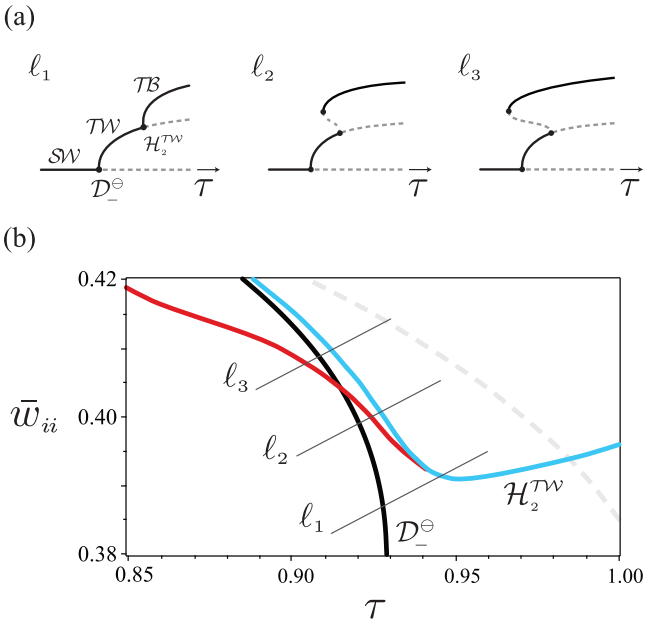

FIG. 10. (a) Schematic bifurcation diagrams along lines ℓ_1, ℓ_2, ℓ_3 as denoted in (b) the $\tau\bar{w}_{ii}$ plane in a subregion of Fig. 9(a). In the bifurcation diagrams, solid black lines denote stable solutions, gray dashed lines denote unstable solutions, and black dots denote bifurcation points. Initials denote different solution branches: $\mathcal{SW}$, stationary bumps; $\mathcal{TW}$, traveling bumps; $\mathcal{TB}$, traveling breathers. The drift bifurcation $\mathcal{D}_-^{\ominus}$ from a $\mathcal{SW}$ to a $\mathcal{TW}$ is supercritical. Numerical simulations suggest that Hopf bifurcation $\mathcal{H}_2^{\mathcal{TW}}$ from a $\mathcal{TW}$ to a $\mathcal{TB}$ is supercritical along line ℓ_1 but subcritical along lines ℓ_2 and ℓ_3 with a stable-unstable pair of $\mathcal{TB}$ instead annihilating in a (presumed) saddle-node bifurcation of traveling breathers (limit cycles) corresponding to the red curve.

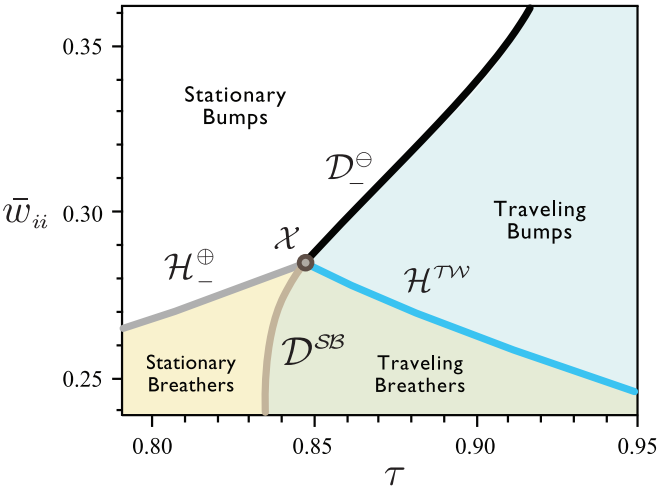

FIG. 11. A hypothetical codimension-2 bifurcation with a mode interaction occurring between the odd $\lambda_{\pm}^{\ominus}$ eigenmode (drift instability) and the even $\lambda_{\pm}^{\oplus}$ eigenmode (Hopf instability) consistent with results in Fig. 9. Curves are denoted as follows: $\mathcal{H}_-^{\oplus}$, curve of Hopf bifurcations of stationary bumps; $\mathcal{D}_-^{\ominus}$, curve of drift bifurcations of stationary bumps; $\mathcal{H}^{\mathcal{TW}}$, curve of Hopf bifurcations of traveling bumps; and $\mathcal{D}^{\mathcal{SB}}$, curve of drift bifurcations of stationary breathers. $\mathcal{H}_-^{\oplus}$, $\mathcal{D}_-^{\ominus}$, and $\mathcal{H}^{\mathcal{TW}}$ are calculated from analytical results. Curve $\mathcal{D}^{\mathcal{SB}}$ is a hypothetical curve of drift bifurcations of stationary breathers consistent with the transition from stationary to traveling breathers (from speed 0) in simulations. Each bifurcation is supercritical with each region denoting the stable attractor.

stationary and traveling types of bumps and breathers. A bifurcation diagram is depicted in Fig. 11 and is structured to be consistent with the stable attractors revealed in the existence equations and simulations in Fig. 9(b). $\mathcal{H}_-^{\oplus}$ denotes a curve of Hopf bifurcations of stationary bumps with respect to the even-symmetric eigenmode. $\mathcal{D}_-^{\ominus}$ denotes a curve of drift bifurcations of stationary bumps with respect to the odd-symmetric eigenmode. $\mathcal{H}^{\mathcal{TW}}$ is a curve of Hopf bifurcations of traveling bumps. $\mathcal{D}^{\mathcal{SB}}$ denotes a (hypothetical) curve of *drift bifurcations* of *stationary breathers* whereby a stable stationary breather destabilizes and gives rise to a stable traveling breather.

The sequence of stable attractors that exchange stability as the bifurcation curves in Fig. 11 are traversed is as follows. Traversing curve $\mathcal{D}_-^{\ominus}$, stable stationary bumps destabilize in a supercritical drift bifurcation giving rise to stable traveling bumps. Subsequently, traversing $\mathcal{H}^{\mathcal{TW}}$ stable traveling waves destabilize in a supercritical Hopf bifurcation that gives rise to stable traveling breathers. Alternatively, traversing $\mathcal{H}_-^{\oplus}$, stable stationary bumps destabilize in a supercritical Hopf bifurcation and give rise to stable stationary breathers. And, subsequently traversing $\mathcal{D}^{\mathcal{SB}}$ stable stationary breathers destabilize in a supercritical drift bifurcation that leads to the same region of stable traveling breathers. Thus, bifurcation points along $\mathcal{D}^{\mathcal{SB}}$ and $\mathcal{H}^{\mathcal{TW}}$ are connected by a sheet of stable traveling breathers bifurcating from these curves. The traveling breathers bifurcating from these curves exhibit two amplitudes, measured as *average wave speed* and *oscillation amplitude*, which vary oppositely between $\mathcal{D}^{\mathcal{SB}}$ and $\mathcal{H}^{\mathcal{TW}}$. In particular, average wave speed $\tilde{c}$ increases from speed 0 when traversing from $\mathcal{D}^{\mathcal{SB}}$ to $\mathcal{H}^{\mathcal{TW}}$, whereas oscillation amplitude $\delta\xi_{e,i}$ decreases to 0 at $\mathcal{H}^{\mathcal{TW}}$. Average wave speed $\tilde{c}$ was defined as the average speed of the center of the activity bump, and oscillation amplitude $\delta\xi_j$ was defined to be half the difference between maximum and minimum widths of the oscillating bump in population $j \in \{e,i\}$.

F. A case of subcritical bifurcations

We now revisit the parameter regime corresponding to the results in Figs. 1 and 2 and consider $\tau < 1.2$, for fixed $\bar{w}_{ii} = 0.24$, to investigate the bifurcation scenario that generates these stable traveling waves that continue for large τ. In Fig. 12(a), the curves of Hopf $\mathcal{H}_-^{\oplus}$ and drift $\mathcal{D}_+^{\ominus}$ bifurcations of stationary bumps are plotted as τ and $\hat{w}_{ii}$ vary in this parameter region. And, as before, in a narrow interval the stationary bump width $\xi_{e,i} \to \infty$ as $\bar{w}_{ii} \nearrow 0.25$ (gray dashed line) with curves $\mathcal{H}_-^{\oplus}$ and $\mathcal{D}_+^{\ominus}$ converging in this limit.

Stable stationary bumps exist to the left of curve $\mathcal{H}_-^{\oplus}$ where they destabilize in a Hopf bifurcation of a stationary bump. For fixed $\bar{w}_{ii} = 0.24$, these stationary bumps are depicted in Fig. 12(b) as the solid and dashed dark blue horizontal curve at speed $c = 0$. At $\tau = \tau_{\text{crit}}^{\mathcal{H}} = 1.058\,23$ the branch of stable stationary bumps destabilizes in a subcritical Hopf bifurcation $\mathcal{H}_-^{\oplus}$ occurring with respect to the even $\lambda_{\pm}^{\oplus}$ eigenmode.

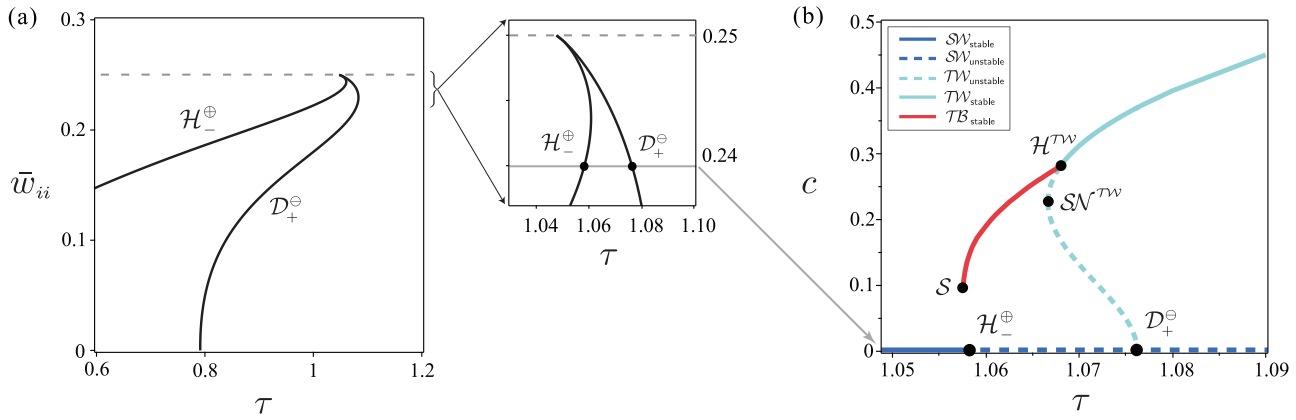

FIG. 12. Bumps and breathers in an different bifurcation scenario involving subcritical bifurcations in a alternate parameter region described in Sec. V F. (a) Curves of Hopf bifurcations $\mathcal{H}_-^{\oplus}$ and drift bifurcations $\mathcal{D}_+^{\ominus}$ of stationary bumps in the $(\tau, \bar{w}_{ii})$ plane, with other parameters as in Figs. 1 and 2. Stationary bumps are stable (unstable) to the left (right) of curve $\mathcal{H}_-^{\oplus}$. (b) Bifurcation diagram for stationary bumps ($\mathcal{SW}$), traveling bumps ($\mathcal{TW}$), and traveling breathers ($\mathcal{TB}$) where the vertical axis measures the traveling wave speed c vs the bifurcation parameter τ for fixed $w_{ii} = 0.24$ [average speed $\tilde{c}$ of the bump center is used in the case of a traveling breather ($\mathcal{TB}$)]. Solid (dashed) curves denote the stable (unstable) solutions.

Numerical simulations suggest that the Hopf bifurcation is subcritical with no sharp transition to a stable stationary breather. Centered (syntopic) perturbations of the unstable stationary bump lead through a transition from growing oscillations, to an epoch where it appeared to spend time near a stationary breather, followed by an abrupt divergence, after the oscillations grew sufficiently large, that ultimately approached a traveling breather. Some perturbations also resulted in a collapse of the activity bump to the rest state. Some offset (allotopic) perturbations to the unstable stationary bump rapidly evolved towards stable traveling breathers, which are discussed further below.

Next, the existence and stability of traveling waves were investigated in the vicinity of curve $\mathcal{D}_+^{\ominus}$ of drift bifurcations of (unstable) stationary bumps ($\lambda_{\pm}^{\oplus}$ eigenmode has a pair of complex eigenvalues with positive real part). For $\bar{w}_{ii} = 0.24$, the translation mode ($\lambda_{\pm}^{\ominus}$) destabilizes in a drift bifurcation at $\tau = \tau_{\text{crit}}^{\mathcal{D}} = 1.076\,21$. In Fig. 12(b), the bifurcation was found to be subcritical, i.e., by solving the existence equations, a branch of unstable traveling waves was found bifurcating from the stationary bump at the drift bifurcation point, with wave speed c increasing from speed $c = 0$ and continuing for $\tau < \tau_{\text{crit}}^{\mathcal{D}}$ where $\lambda_+^{\ominus} < 0$. The Evans function reveals this branch is unstable due to a positive real eigenvalue and a pair of complex eigenvalues with positive real part. The branch terminates in a saddle-node bifurcation $\mathcal{SN}^{\mathcal{TW}}$ of traveling bumps ($\mathcal{TW}$) at $\tau \approx 1.066\,65$ with an upper branch (larger speed c) of coexistent traveling bumps that includes the stable traveling bumps shown in Fig. 1 for $\tau \geqslant 1.2$. This upper branch is unstable from $\mathcal{SN}^{\mathcal{TB}}$ to $\tau \approx 1.068\,05$ where a Hopf bifurcation of a traveling bump $\mathcal{H}^{\mathcal{TW}}$ occurs, rendering the branch of traveling bumps stable for $\tau > 1.068\,05$.

The Hopf bifurcation of a traveling bump $\mathcal{H}^{\mathcal{TW}}$ was determined to be supercritical from extensive numerical simulations in the vicinity of the bifurcation point. The oscillation amplitude of the traveling breathers bifurcating from the traveling bumps increases from amplitude 0 as τ decreases from 1.068 05 as illustrated in Fig. 13. Moreover, the average speed $\tilde{c}$ of the traveling breathers decreases from the same speed c as the traveling wave at the bifurcation point $\mathcal{H}^{\mathcal{TW}}$ as seen in the red curve in Fig. 12. The branch of traveling breathers was continued to $\tau \approx 1.057\,65$, denoted by point $\mathcal{S}$ in Fig. 12(b) where the traveling breather appears to vanish, ostensibly in a saddle-node bifurcation of traveling breathers. Traveling breathers exhibit two amplitudes (average wave speed $\tilde{c}$ and oscillation amplitude $\delta\bar{w}_{e,i}$) which vary oppositely along this curve. In particular, average wave speed $\tilde{c}$ increases while oscillation amplitude $\delta\bar{w}_{e,i}$ decreases when traversing from $\mathcal{S}$ to $\mathcal{H}^{\mathcal{TW}}$.

In Fig. 14, two simple bifurcation diagrams are posed that could connect the bifurcation structure around the branch of traveling breathers in Fig. 12; other explanations naturally exist. The proposed diagrams fill in the missing structure by building on the notion that a traveling breather could bifurcate from a stationary breather in a drift bifurcation, for which we found evidence in Fig. 9. Simulations suggested that the Hopf bifurcation of the stationary bump was subcritical. If the

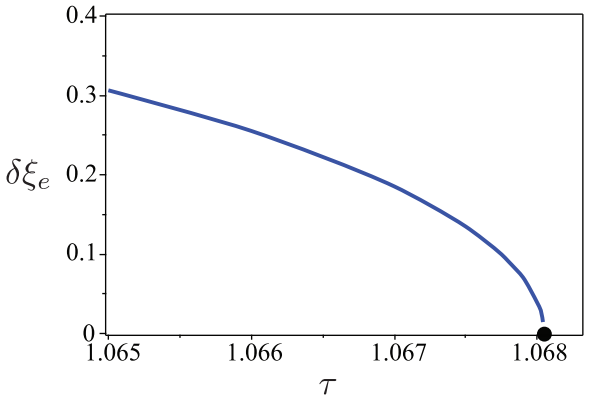

FIG. 13. The oscillation amplitude $\delta\xi_e$ of the time-varying width of the traveling breather $\mathcal{TB}$ (red curve) in Fig. 12 plotted as τ varies from 1.065 to $\tau \approx 1.068\,05$ (large dot) which coincides with the Hopf bifurcation point $\mathcal{H}^{\mathcal{TW}}$ occurring on the branch of traveling bumps $\mathcal{TW}$. This is consistent with a supercritical bifurcation giving rise to a branch of stable traveling breathers emerging at the bifurcation point.

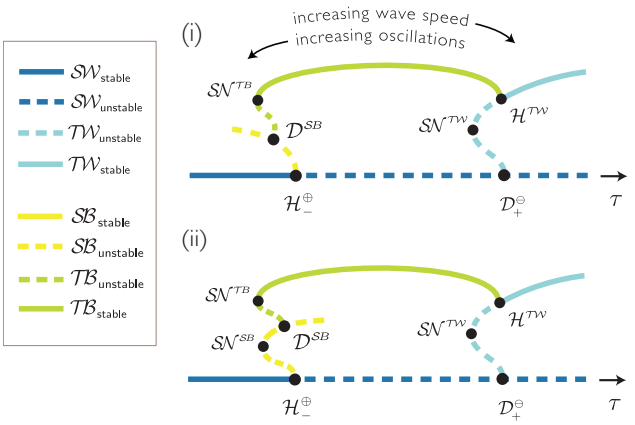

FIG. 14. Two hypothetical (schematic) bifurcation diagrams that may connect the structure of the stable attractors found the in analytical calculations and simulations in Fig. 12(b). Different solution types are denoted by colors and symbols: $\mathcal{SW}$, stationary bump (wave); $\mathcal{TW}$, traveling bump (wave); $\mathcal{SB}$, stationary breather; and $\mathcal{TB}$, traveling breather. The solid (dashed) curves indicate the stable (unstable) solutions. The vertical axis abstractly represents the amplitude of the bifurcating solutions from the stationary bump (amplitude 0) and, in the traveling breather case, represents a mix of wave speed and oscillation amplitude. Symbols $\mathcal{SN}^{\mathcal{X}}, \mathcal{H}^{\mathcal{X}}, \mathcal{D}^{\mathcal{X}}$ denote saddle-node, Hopf, and drift bifurcation, respectively, occurring on a solution (or solution pair) of type $\mathcal{X}$. Points $\mathcal{H}^{\oplus}_{-}$ and $\mathcal{D}^{\ominus}_{+}$ along the branch of stationary bumps ($\mathcal{SW}$) denote the points of Hopf and drift bifurcation as τ is varied. In simulations of stable traveling breathers (Figs. 12 and 13), the average wave speed $\tilde{c}$ increases as τ increases from $\mathcal{SN}^{\mathcal{TB}}$ to $\mathcal{H}^{\mathcal{TW}}$ whereas the oscillation amplitude $\delta\xi_j$ (breathing) increases from amplitude 0 as τ *decreases* from $\mathcal{H}^{\mathcal{TW}}$ to $\mathcal{SN}^{\mathcal{TB}}$. The hypothetical component is the connection from the curve of stable traveling breathers ($\mathcal{TB}$) to the Hopf bifurcation $\mathcal{H}^{\oplus}_{-}$.

traveling breathers subsequently bifurcate from an unstable stationary breather, it is presumed that the drift bifurcation is subcritical (i) because the branch of traveling breathers at point $\mathcal{S}$ in Fig. 12 appears to emerge at a nonzero average wave speed $\tilde{c}$ rather than 0 and (ii) to be consistent with the principle of exchange of stability.

VI. DISCUSSION

In this paper, we have developed analytical conditions for the existence and stability of traveling bump solutions in an E-I neural field. The existence conditions form a 4D system of nonlinear equations that can be solved numerically but depart from many previous studies of traveling waves in neural fields which enjoy existence equations as 2D nonlinear systems whose solutions can be visualized as intersection points of zero sets in a plane. As parameters are varied, solutions in the 4D system can be traced out via numerical continuation from a known solution that can be discovered in various ways, including a good initial guess that converges in a numerical solver, approximate solutions found in numerical simulations, and expected solutions in the vicinity of drift bifurcations of stationary bumps. Identifying the point spectrum using the Evans function is analogous to previous studies by identifying intersections of the zero sets of its real and imaginary parts; the natural complication of the higher-dimensional (4×4) determinant than in previous studies renders calculation of the zero sets more computationally intensive at high resolution. Good agreement was found between the numerical results of analytic calculations and the results of numerical simulations of the E-I neural field (1) where stable traveling bumps exist.

Existence and stability conditions were found to reduce in the limit of wave speed $c \to 0$ to the equivalent conditions for stationary bumps developed in [23,52]. These conditions were then used to investigate drift and Hopf bifurcations of stationary bumps. We advance the notion of the drift bifurcation of a stationary bump (i.e., a pitchfork bifurcation occurring with respect to the translation mode of the linearization) as a natural mechanism for generating traveling waves in E-I neural fields. Although drift bifurcations could conceivably arise from varying any system parameters, we showed that the relative inhibitory time constant τ is naturally conducive to producing drift bifurcations and that the translation mode always destabilizes at a positive critical value of τ.

To obtain a more global perspective of the dynamics of localized solutions in E-I neural fields, we combined the analytically determined existence and stability conditions of both traveling and stationary bumps with numerical simulations to explore the different stable attractors and their bifurcations in different regions of the $\tau\bar{w}_{ii}$-parameter plane delineated by curves of drift and Hopf bifurcations of stationary bumps and Hopf bifurcations of traveling bumps. We found evidence for both supercritical and subcritical Hopf bifurcations of traveling bumps that give rise to stable traveling breathers and, in certain regions, bistability with stable stationary or traveling bumps. We also found evidence for a codimension-2 *drift-Hopf* bifurcation which acts as an organizing center for four kinds of solutions: stationary bumps, traveling bumps, stationary breathers, and traveling breathers.

The two parameters τ and $\bar{w}_{ii}$ that were varied embody different aspects of the dynamics of the inhibitory population, with τ affecting the temporal response of inhibition to its inputs and $\bar{w}_{ii}$ modulating the strength of self-inhibition. Both affect the ability for the inhibitory population to control the spread of excitation in different ways. Indeed, increasing $\bar{w}_{ii}$ sufficiently high results in an I population that is unable to control the spread of excitation from usurping the domain as the system approaches the uniformly excited state. For $\bar{w}_{ii}$ below this level, excitation can be controlled if the inhibitory dynamics are sufficiently fast (smaller τ), whereas, as τ increases the system is naturally attracted to traveling breathers in the form of oscillatory activity bumps whose flare up of activity increases as the self-inhibition increases. For moderate $\bar{w}_{ii}$, there is an interval of self-inhibitory strengths where stable stationary bumps occur for sufficiently fast inhibition, otherwise traveling bumps occur where the slower inhibition allows the activity bump to propagate but prevents excitation from growing uncontrollably. When self-inhibition is sufficiently decreased, an imbalance occurs resulting in an oscillatory interplay between excitation and inhibition in the form of stationary or traveling breathers (depending on the relative time constant τ). As the excitation widens, inhibition is recruited; in turn, the enhanced inhibition now diminishes the excitation which leads to a subsequent decrease in inhibition, with this cycle repeating. For sufficiently weak self-inhibition,

the inhibition strongly controls excitation and extinguishes it, with the network returning to the rest state unless inhibition is sufficiently slow (large τ) to allow excitation to propagate as traveling waves. Thus, the strength $\bar{w}_{ii}$ of I-to-I synaptic connections can tightly control the stability of stationary and traveling bumps by regulating the recruitment of activity in the I population.

To investigate other bifurcation mechanisms underlying the emergence of traveling waves and breathers in the E-I neural field, we further examined a different region of parameter space and showed that, as the relative inhibitory time constant τ is varied, subcritical bifurcations of stationary bumps and secondary bifurcations can give rise to an interval of traveling breathers that bridges the gap between two separated regions of stable stationary and traveling bumps. This result combined with the previous results presents a variety of combinations of drift, Hopf, and saddle-node bifurcations capable of generating stable traveling waves and breathers.

We note that two differences between the E-I neural field considered herein [23] and the neural field analyzed in [22] are that the latter contains no self-inhibition (I-to-I) and the I-to-E synaptic interaction is linear. The results discussed here elucidate some of the roles self-inhibition plays in regulating the dynamics of stationary and propagating localized activity. We also note that the eigenvalues of the rest state of the E-I neural field are always real in contrast to [29] where the complex eigenvalues of the rest state lead to richer behavior. Given the large number of parameters in E-I neural field (1) one expects many bifurcation scenarios to occur in different regions of parameter space. In this paper, we have described how varying the relative inhibitory time constant and I-to-I synaptic strength can lead traveling waves and breathers in a particular region in parameter space. In the case of inputs these results would be valid in regions where the input is uniformly close to zero and the excitatory synaptic connections decay sufficiently fast. Note that in a purely inhibitory sparse network of spiking neurons, the number and strength of I-to-I synaptic connections over a range were found to play a role in supporting stable synchronous activity [56].

Advances in voltage-sensitive dyes [4,6], local field potential (LFP) recordings [10], and calcium-epifluorescence imaging [57] are beginning to reveal the spatiotemporal dynamical patterns generated by neural tissue *in vivo* and *in vitro* under different conditions. Developing an understanding of the different spatiotemporal patterns these networks support is one of the current objectives of neural field theory, which provides a more analytically tractable framework for describing the activity large neuronal populations. Our results reveal how the basic connectivity of E-I networks are capable of supporting localized stationary, traveling, and oscillatory activity bumps. If network parameters are modulated by different neuronal processes in time or across space, this could permit the network to switch between these different states that maintain activity in stationary, propagating and/or oscillatory form, allowing the same network to perform different tasks. Moreover, oscillations have been found in many regions of neocortex and thalamus and may play an important role in synchronizing activity between different layers or brain regions [58,59]; breathers may be one type of spatiotemporal structure such oscillations could exhibit.

[1] Y. Chagnac-Amitai and B. W. Connors, J. Neurophysiol. **61**, 747 (1989).
[2] R. B. Langdon and M. Sur, J. Neurophysiol. **64**, 1484 (1990).
[3] J.-Y. Wu, L. Guan, and Y. Tsau, J. Neurosci. **19**, 5005 (1999).
[4] A. Benucci, R. A. Frazor, and M. Carandini, Neuron **55**, 103 (2007).
[5] J.-Y. Wu, X. Huang, and C. Zhang, The Neuroscientist **14**, 487 (2008).
[6] W. Xu, X. Huang, K. Takagaki, and J.-Y. Wu, Neuron **55**, 119 (2007).
[7] K. Takagaki, C. Zhang, J.-Y. Wu, and M. T. Lippert, Neurosci. Lett. **431**, 191 (2008).
[8] T. Sato, I. Nauhaus, and M. Carandini, Neuron **75**, 218 (2012).
[9] L. Muller and A. Destexhe, J. Physiol. (Paris) **106**, 222 (2012).
[10] I. Nauhaus, L. Busse, D. L. Ringach, and M. Carandini, J. Neurosci. **32**, 3088 (2012).
[11] T. P. Zanos, P. J. Mineault, K. T. Nasiotis, D. Guitton, and C. C. Pack, Neuron **85**, 615 (2015).
[12] H. Zhang and J. Jacobs, J. Neurosci. **35**, 12477 (2015).
[13] Z. Yang, D. J. Heeger, R. Blake, and E. Seidemann, J. Neurophysiol. **113**, 277 (2015).
[14] D. J. Pinto, S. Patrick, W. Huang, and B. Connors, J. Neurosci. **25**, 8131 (2005).
[15] K. A. Richardson, S. J. Schiff, and B. J. Gluckman, Phys. Rev. Lett. **94**, 028103 (2005).
[16] H. R. Wilson and J. D. Cowan, Kybernetik **13**, 55 (1973).
[17] G. B. Ermentrout, Rep. Prog. Phys **61**, 353 (1998).
[18] G. Deco, V. K. Jirsa, P. A. Robinson, M. Breakspear, and K. Friston, PLoS Comput. Biol. **4**, e1000092 (2008).
[19] P. C. Bressloff, J. Phys. A: Math. Theor. **45**, 033001 (2011).
[20] P. C. Bressloff, *Waves in Neural Media*, Lecture Notes on Mathematical Modeling in the Life Sciences (Springer-Verlag, New York, 2014).
[21] S.-I. Amari, Biol. Cybern. **27**, 77 (1977).
[22] D. J. Pinto and G. B. Ermentrout, SIAM J. Appl. Math. **62**, 226 (2001).
[23] P. Blomquist, J. Wyller, and G. Einevoll, Physica D **206**, 180 (2005).
[24] D. J. Pinto and G. B. Ermentrout, SIAM J. Appl. Math. **62**, 206 (2001).
[25] L. Zhang, Chin. Annal. Math. **22**, 343 (2001).
[26] S. Coombes and M. Owen, Differ. Integr. Eqn. **16**, 513 (2004).
[27] S. E. Folias and P. C. Bressloff, SIAM J. Appl. Math. **65**, 2067 (2005).
[28] D. J. Pinto, R. Jackson, and C. Wayne, SIAM J. Appl. Dyn. Syst. **4**, 954 (2005).
[29] W. C. Troy and V. Shusterman, SIAM J. Appl. Dyn. Syst. **6**, 263 (2007).
[30] B. Sandstede, Int. J. Bifurcation Chaos **17**, 2693 (2007).
[31] W. C. Troy, SIAM J. Appl. Dyn. Syst. **7**, 1247 (2008).
[32] G. Faye, SIAM J. Appl. Dyn. Syst. **12**, 2032 (2013).
[33] Z. P. Kilpatrick and P. C. Bressloff, Physica D **239**, 547 (2010).

[34] H. G. E. Meijer and S. Coombes, J. Math. Biol. **68**, 1249 (2013).
[35] A. Hutt and F. M. Atay, Phys. Rev. E **73**, 021906 (2006).
[36] H. G. E. Meijer and S. Coombes, EPJ Nonlin. Biomed. Phys. **2**, 3 (2014).
[37] J. Jalics, Physica D **192**, 95 (2004).
[38] P. C. Bressloff, Physica D **155**, 83 (2001).
[39] Z. P. Kilpatrick, S. E. Folias, and P. C. Bressloff, SIAM J. Appl. Dyn. Syst. **7**, 161 (2008).
[40] P. C. Bressloff and S. R. Carroll, PLoS Comput. Biol. **11**, e1004545 (2015).
[41] C. R. Laing, Uncertainty Biol., **17** 367 (2016).
[42] P. C. Bressloff and M. A. Webber, J. Comput. Neurosci. **32**, 233 (2011).
[43] Z. P. Kilpatrick, Phys. Rev. E **89**, 022706 (2014).
[44] Z. P. Kilpatrick and P. C. Bressloff, Physica D **239**, 1048 (2010).
[45] S. E. Folias and G. B. Ermentrout, SIAM J. Appl. Dyn. Syst. **11**, 895 (2012).
[46] C. R. Laing and S. Coombes, Network **17**, 151 (2006).
[47] S. Coombes, H. Schmidt, and D. Avitabile, in *Neural Fields*, edited by S. Coombes, P. beim Graben, R. Potthast, and J. Wright (Springer, New York, 2014), Chap. 7, pp. 187-211.
[48] Z. P. Kilpatrick and G. Faye, SIAM J. Appl. Dyn. Syst. **13**, 830 (2014).
[49] P. C. Bressloff, S. E. Folias, A. Prat, and Y.-X. Li, Phys. Rev. Lett. **91**, 178101 (2003).
[50] S. E. Folias, SIAM J. Appl. Dyn. Syst. **10**, 744 (2011).
[51] G. Faye and J. Touboul, SIAM J. Appl. Math. **74**, 1657 (2014).
[52] S. E. Folias (unpublished).
[53] D. Golomb and G. B. Ermentrout, Proc. Natl. Acad. Sci. USA **96**, 13480 (1999).
[54] Y. Lu, Y. Sato, and S.-I. Amari, Neural Comput. **23**, 1248 (2011).
[55] J. Goulet and G. B. Ermentrout, Biol. Cybern. **105**, 253 (2011).
[56] D. Golomb and D. Hansel, Neural Comput. **12**, 1095 (2000).
[57] T. Berger, A. Borgdorff, S. Crochet, F. B. Neubauer, S. Lefort, B. Fauvet, I. Ferezou, A. Carleton, H. R. Lüscher, and C. C. H. Petersen, J. Neurophysiol. **97**, 3751 (2007).
[58] J. W. Yang, S. An, J. J. Sun, and V. Reyes-Puerta, Cereb. Cortex **23**, 1299 (2012).
[59] Y. Xiao, X.-Y. Huang, S. Van Wert, E. Barreto, J.-Y. Wu, B. J. Gluckman, and S. J. Schiff, Eur. J. Neurosci. **36**, 2201 (2012).